Clim Dyn (2016) 47:2373–2395
DOI 10.1007/s00382-015-2969-3

Predictable signals in seasonal mean soil moisture simulated with observation-based atmospheric forcing over China

Kairan Ying[1] · Tianbao Zhao[1] · Xiaogu Zheng[1] · Xiao-Wei Quan[2] · Carsten S. Frederiksen[3] · Mingxing Li[1]

Received: 30 July 2015 / Accepted: 29 December 2015 / Published online: 12 January 2016

Abstract The Community Land Model version 3.5 is driven by an observation-based meteorological dataset to simulate soil moisture over China for the period 1951–2008. A method for identifying the patterns of interannual variability that arise from slow (potentially predictable) and intraseasonal (unpredictable) variability is also applied; this allows identification of the sources of the predictability of seasonal soil moisture in China, during March–April–May (MAM), June–July–August (JJA), September–October–November (SON) and December–January–February (DJF). The potential predictability (slow-to-total) of the soil moisture above 1 m is high, with lowest value of 0.76 in JJA and highest value of 0.94 in DJF. The spatial distribution of the potential predictability comprises a northwest–southeast gradient, with a minimum center over East China and a maximum center over the northwest. The most important source of predictability is from the soil moisture persistence, which generally accounts for more than 50 % of the variability in soil moisture. The SSTs in the Indian Ocean, the North Atlantic and the eastern tropical Pacific Oceans are also identified as important sources of variability in the soil moisture, during MAM, JJA and SON/DJF, respectively. In addition, prolonged linear trends in each season are an important source. Using the slow principal component time series as predictands, a statistical scheme for the seasonal forecasting of soil moisture across China is developed. The prediction skills, in terms of the percentage of explained variance for the verification period (1992–2008), are 59, 51, 62 and 77 % during MAM–DJF, respectively. This is considerably higher than a normal grid prediction scheme.

Keywords Predictable signal · Weather noise · Potential predictability · Prediction skill

✉ Tianbao Zhao
zhaotb@tea.ac.cn

[1] Key Laboratory of Regional Climate-Environment Research for East Asia, Institute of Atmospheric Physics, Chinese Academy of Sciences, P. O. Box 9804, Beijing 100029, China

[2] Cooperative Institute for Research in Environmental Sciences, University of Colorado at Boulder and NOAA/ESRL/PSD, Boulder, CO, USA

[3] The Bureau of Meteorology, Melbourne, Australia

1 Introduction

Soil moisture is an important component of the climate system, as it can modulate the land surface water, energy and biogeochemical cycles. Changes in soil moisture directly affect plant water availability; in turn, this constrains plant transpiration and photosynthesis, with consequent impacts on plant productivity and crop yields. As the underlying surface condition, soil moisture is a key variable for atmospheric and climate processes through land–atmosphere interactions, in particular for precipitation and radiation anomalies. Because of the influences of soil moisture conditions on agriculture, hydrology and climate, skillful seasonal forecasts of soil moisture have obvious potential benefits for predicting other short-term climate variations and for practical applications, such as agricultural drought assessments and ecosystem management.

Several studies have investigated the spatial and temporal characteristics of China's soil moisture variability and its long-term trends (e.g. Ma et al. 2000, 2001; Nie et al. 2008; Zhang et al. 2008a, b; Zuo and Zhang 2009; Li et al.

2010, 2011, Li and Ma 2012). Because of the strong "memory" of soil moisture (Koster and Suarez 2001; Seneviratne et al. 2006, 2010), soil moisture is one of the chief sources of forecast skill for summer precipitation over East China through surface energy balance processes (e.g. Sun et al. 2005; Zuo and Zhang 2007; Zhan and Lin 2011; Zhang and Zuo 2011; Meng et al. 2014). Soil moisture also plays an important role in characterizing prolonged droughts in China (Wang et al. 2011). These results suggest that it is possible for soil moisture to have a larger potential predictability than atmospheric variables, as it can "remember" wet or dry anomalies long after the conditions responsible for those anomalies are forgotten by the atmosphere. A few important questions still remain unanswered regarding the application of soil moisture to climate predictions for China. Firstly, it is unclear how large the potential predictability of seasonal mean soil moisture is in China. Also, little is known about the best possible predictors that can generate skillful predictions for the seasonal mean soil moisture in China. The purpose of this study was to address these questions. In particular, we have attempted to obtain a detailed understanding of the processes that control the interannual variability of the seasonal mean soil moisture.

In order to explore the potential predictability of seasonal mean fields, Zheng and Frederiksen (2004; hereafter ZF2004) developed a methodology for estimating the spatial patterns of the intraseasonal and slow components from monthly mean data. The intraseasonal component is considered to be the "weather noise component" (Madden 1976; Zheng and Frederiksen 1999; Zheng et al. 2000) and is essentially unpredictable a season or more ahead. Predictable signals are kept in the slow component, which is related to processes that are fairly constant over the season and themselves potentially predictable [such as sea surface temperature (SST)]. By separating out the weather-noise, the predictability of the slow component is generally better than the predictability of the original seasonal mean in two aspects: (1) the temporal variation of the slow component generally has larger potential predictability (expressed as the ratio of the variance of the slow component and the total variance); and (2) the temporal variation of the slow component is likely to be better related to slowly varying external forcings and slowly varying internal variability (ZF2004). This method has been previously applied in studies of predictable signals for seasonal rainfall (e.g. Zheng and Frederiksen 2006; Frederiksen et al. 2014; Ying et al. 2013, 2015), temperature (e.g. Grainger et al. 2009), and geopotential height (e.g. Frederiksen and Zheng 2000, 2004, 2007; Grainger et al. 2013; Ying et al. 2014).

In this study, we applied the ZF2004 variance decomposition method to monthly mean soil moisture data obtained from a simulation with the Community Land Model and observation-based atmospheric forcing over China. Our objective here is to better understand the possible sources of potential predictability of seasonal mean soil moisture in China. We also made an effort to construct a statistical seasonal prediction scheme. Data and methodology used are described in Sects. 2 and 3; analyses of the most predictable signals and their possible sources are presented and discussed in Sect. 4; the proposed prediction scheme is presented in Sect. 5; some analysis of the unpredictable modes is presented in Sect. 6; and conclusions and discussions are given in Sect. 7.

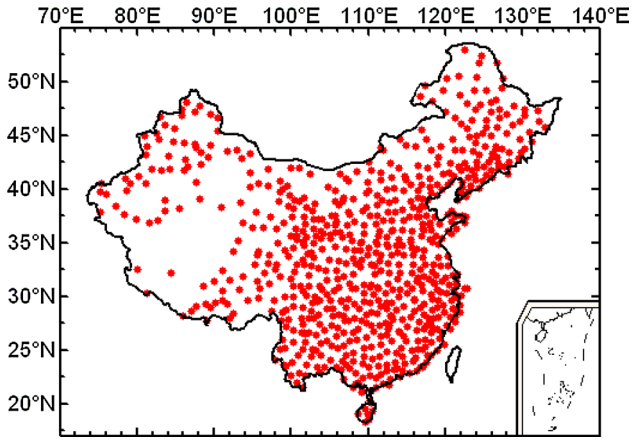

Fig. 1 The Chinese meteorological stations (740 total) from which the ObsFC forcing data were generated

2 Data

2.1 Soil moisture

Since the observational datasets of soil moisture in China are scarce and limited in space and time, numerical model simulations have been used as a source of soil moisture information for climate studies (e.g. Sheffield et al. 2004; Sheffield and Wood 2007; Wang et al. 2011). In this paper, the soil moisture variables, used to identify the predictable signals and their associated predictors, were sourced from an offline simulation using Community Land Model version 3.5 (CLM3.5; Oleson et al. 2007), released by the National Center for Atmospheric Research (NCAR). Details of the model's structure and physical processes can be found in the references above. To simulate soil moisture over China, the CLM3.5 was driven by a set of observation-based meteorological forcings (hereafter ObsFC), including precipitation, air temperature, pressure, specific humidity, wind speed and radiation. In particular, the observed air temperature, wind speed, precipitation and surface pressure data were obtained from 6-hourly station observations at 740 routine Chinese meteorological stations

(Fig. 1), during 1951–2008. The specific humidity was calculated from dry and wet bulb temperatures for the same 58-year period. The observation dataset was provided by the China Meteorological Administration (CMA) and had undergone a series of quality controls (QC), including checks for extreme values and internal consistency (e.g. duplicate data and position, incorrect units, and data coding, among others), and removal of questionable data (Zhai et al. 2005; Yu et al. 2007; Shen et al. 2010). To establish the ObsFC data, these in situ observational variables were firstly downscaled from 6- to 3-hourly resolutions, using simple linear interpolations, while retaining the observational daily, monthly and annual totals. The 3-hourly in situ data were then downscaled to a spatial resolution of approximately 0.5° × 0.5°, using the kriging interpolation technique (Goovaerts 1997; Hunter and Meentemeyer 2005); elevation adjustments were performed for the temperature and pressure fields, following the methods of Zhao et al. (2008) and Zhao and Hua (2009). The radiation flux, with a time span of 58 years from 1951 to 2008, was taken from Princeton's dataset (Sheffield et al. 2006), because of the short time span and sparse spatial distribution of the observations. The Princeton's dataset was constructed by combining a suite of global observation-based datasets with the National Centers for Environmental Prediction-National Center for Atmospheric Research (NCEP–NCAR) reanalysis (Kalnay et al. 1996), which has a horizontal resolution of 1° × 1° and a temporal resolution of 3 h. In this study, Princeton's radiation data were firstly interpolated to approximately 0.5° horizontal resolution, using a bilinear interpolation method. Then, the data within the study domain were extracted. We note that, over the western Tibetan Plateau, the observational stations are sparse; as such, the atmospheric forcing was likely less reliable over this region.

Our simulations were performed using a 3-h step and approximately 0.5° spatial resolution. To eliminate the model initialization effects, the CLM3.5 was first run for 400 year by cycling the 1951–2000 forcing data. The CLM3.5 was then run from 1951 to 2008, having been initialized with the final year of the spin-up run, to construct the soil moisture data across China (hereafter referred to as CLM3.5/ObsFC). The units of the simulated soil moisture (CLM3.5/ObsFC) are m^3 water/m^3 soil; that is, the amount of soil water relative to the observed local soil capacity. The total 0–3.43 m soil column was divided into ten layers, with an increasing thickness from the upper to lower layers. In this study, we were mainly interested in the soil moisture in the uppermost 1 m (top-1 m), as it clearly reflects the climate conditions. Therefore, the soil moisture was vertically integrated through the layers 7, 28, 62, 119, 212, 366, 620 and 1040 mm; the units of this vertically integrated soil moisture are mm. We also analyzed the soil moisture in the top 10 cm (top-10 cm; vertically integrated through the 7, 28, 62 and 119 mm layers), to assess the quality of our CLM3.5/ObsFC simulation, as there were more soil moisture in situ observations in the top layer. In addition, in order to understand how the potential predictability and the predictable patterns changed with depth, we further analyzed the soil moisture at different levels, between 0.007 and 1.040 m depth, across China.

In order to evaluate the simulated and predicted CLM3.5/ObsFC soil moisture data sets for China, we used the in situ observed soil moisture data across China, during the verification period comprising 1992–2008; this data comprised a network of 778 agricultural meteorological stations located in mainland China and was provided by the CMA National Meteorological Information Center (NMIC). The soil moisture observations were measured every 10 days (generally on the 8th, 18th and 28th day of each month), at soil depths of 10, 20, 30, 40, 50, 70 and 100 cm. No measurements were recorded in frozen soil. As the soil moisture observation data were mainly used for agriculture, they were expressed as the relative soil moisture content (%); that is, the ratio of soil moisture content (mass percentage of soil water in dry soil) to the field capacity. Monthly mean observational soil moisture data for each month was calculated as the average from the n (n = 1, 2 or 3; depend on observation times in a specific month)-days of measurements. We calculated the measuring frequency of the monthly mean soil moisture for China and selected 142 (46) stations from the 778 stations, which had more than 75 % (50 %) of the observational times during March to November, in the period 1992–2008, for the top-10 cm (top-1 m) soil moisture layers. In order to clearly compare between the observations and the simulations, the monthly means of the CLM3.5/ObsFC simulation was also defined as a n (n = 1, 2, or 3)-days average, consistent with the observation data. However, when analyzing the potential predictability and predictable modes of the soil moisture in China, the monthly means of the CLM3.5/ObsFC simulation were calculated as the averages of all the days in each month.

To compare the spatial distributions and temporal variations, between the simulations and in situ observations of soil moisture in China, we calculated the climatological means and variances of the simulated and station observed soil moisture in China, between March and November, during the period 1992–2008 (Fig. 2, left and middle columns). In general, for both the top-1 m and top-10 cm soil moisture, the climatological means displayed a similar east–west spatial gradient in the simulations and observations (left column of Fig. 2). Specifically, the northwest, including most of Xingjiang, western Gansu, Inner Mongolia and northern part of Qinghai-Tibetan Plateau, previously identified as the arid and semiarid areas of China

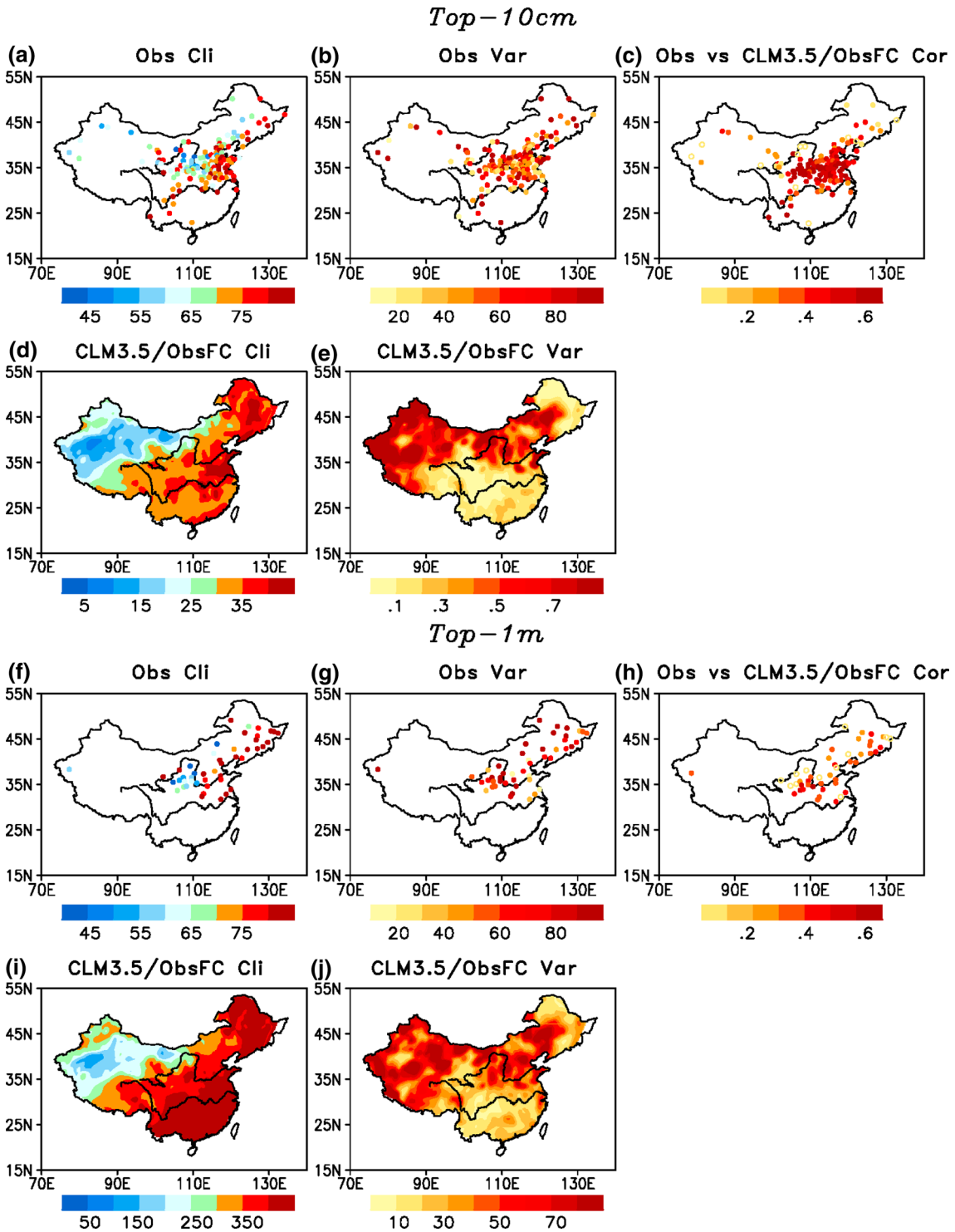

Fig. 2 Spatial distributions of the **a**–**e** top-10 cm and **f**–**j** top-1 m soil moisture climatology means (*left column*; **a**, **d**, **f**, **i**) and variances (*middle column*; **b**, **e**, **g**, **j**) of the observed data (**a**, **b**, **f**, **g**; unit: %) and CLM3.5/ObsFC simulated data (**d**, **e**, **i**, **j**; unit: mm); and the correlation (*right column*; **c**, **h**) between the soil moisture monthly mean observations and the CLM3.5/ObsFC simulations, during the period 1992–2008 (March to November). *Solid cycles* indicate correlation coefficients significant above 95 % confidence level according to the Student *t* test

(Zhao et al. 2014), was relatively drier than the eastern parts of China, especially the regions over northeastern China and central eastern China close to the region of Yangtze–Huaihe river valley (YH), which is the region most influenced by the East Asian Monsoon (EAM) (Wang and LinHo 2002). In terms of the soil moisture interannual variability, the CLM3.5/ObsFC simulations show that large amplitude centers were mainly located in the northern part of China (Fig. 2e, j), which is generally consistent with the analysis of the in situ soil moisture observations (Fig. 2b, g). The point-wise correlations between the simulated and observed soil moisture are shown in the right column of Fig. 2; for each station location, a linear interpolation was done for the gridded CLM3.5/ObsFC simulation data, to interpolate from the grid to the station. The seasonal cycle of the data was removed before the correlation calculations. The monthly correlations have enormous regional differences, which is higher in the east [with an average of about 0.6(/0.4) for top-10 cm(/top-1 m) soil moisture] than the west. This is mainly because the station observations are most continuous in space and time over eastern China but distribute sparsely in western China, especially over the western Tibetan Plateau. Generally, the CLM3.5/ObsFC simulations well captured the historical temporal characteristics of the soil moisture in China.

2.2 Sea surface temperature

To help identify important interannual SST relationships with the atmospheric circulation and soil moisture patterns, we have used the monthly mean SSTs from the UK Meteorological Office Hadley Centre 1° × 1° (latitude/longitude grid) HADISST1.1 dataset (Rayner et al. 2003) from October 1950 to December 2008. The area used to produce the one-point correlation maps in this paper is between 60°S and 60°N.

2.3 Precipitation, temperature and wind speed

The monthly precipitation and temperature datasets used in this study are from a network of 160 stations in China for the period of 1951–2008, supplied by the CMA National Climate Center. The monthly mean 2 m wind speed is obtained from the CMA NMIC, from a network of 148 stations in China for the same 58 years.

2.4 Reanalysis data

The monthly mean geopotential height at 500 hPa is derived from the NCEP–NCAR reanalysis (Kalnay et al. 1996) for the period 1951–2008, which has a horizontal resolution of 2.5° × 2.5°.

3 Methodology

3.1 Identifying predictable and intraseasonal modes

The interested readers are referred to ZF2004 and Frederiksen and Zheng (2007) for a detailed description of the underlying ideas and description of the methodology. Here, we just give a brief introduction of this method. Let x_{ym} represents monthly values of a climate variable in month m ($m = 1, 2, 3$; m is in a specific season) and in year y ($y = 1,\ldots,$ Y, where Y is the total number of years). After removing the annual cycle from the data, x_{ym} is conceptually decomposed into two components consisting of a seasonal "population" mean (μ_y) and a residual departure from this mean (ε_{ym}), that is,

$$x_{ym} = \mu_y + \varepsilon_{ym} \tag{1}$$

Equation (1) implies that month-to-month fluctuations, or intraseasonal variability, arises entirely from ε_{ym} ($m = 1, 2, 3$). If we let "o" representing an average taken over an independent variable (i.e., m or y), a sample seasonal mean can then be written as

$$x_{yo} = \mu_y + \varepsilon_{yo} \tag{2}$$

where ε_{yo} is the intraseasonal or unpredictable component, as it is associated with intraseasonal variability, which is unpredictable on interannual, or longer, timescales. While μ_y is associated with the interannual variability of external forcing and slowly varying internal dynamics, and it is referred to as the potentially predictable component. In ZF2004 approach, the covariance matrix between two slow or predictable components can be estimated as

$$V\left(\mu_y, \mu'_y\right) = V\left(x_{yo}, x'_{yo}\right) - V\left(\varepsilon_{yo}, \varepsilon'_{yo}\right), \tag{3}$$

where the first term can be calculated directly from two seasonal means, and second term that represents the interannual covariance of the intraseasonal components can be estimated by monthly mean data as in ZF2004. Once the intraseasonal and slow covariance matrices of the seasonal mean soil moisture have been estimated by ZF2004 decomposition method, an empirical orthogonal function (EOF) analysis is applied to identify the leading modes of each covariance matrix. For convenience, we shall refer to the EOFs of the slow (/intraseasonal) covariance matrices as the predictable or slow modes (/unpredictable or intraseasonal modes) of interannual variability in the seasonal mean soil moisture. The corresponding principal component (PC) time series of each predictable mode is obtained by projecting the field of seasonal mean soil moisture anomalies onto the corresponding EOF mode for each season and year in the time series.

Table 1 Variability of the total, slow and intraseasonal components of seasonal soil moisture in the top-1 m soil depth in China (unit: mm^2) and the potential predictability of seasonal soil moisture in the top-1 m soil depth in China, expressed as the ratio of slow to total variance (S/T) for the period 1951–2008

Season	Total Var.	Slow Var.	Intra Var.	S/T
MAM	71,116	59,980	11,136	0.84
JJA	111,850	84,754	27,096	0.76
SON	99,785	89,095	10,690	0.89
DJF	69,500	65,078	4422	0.94

3.2 Potential predictability

The *potential predictability* of the seasonal mean field (i.e., seasonal mean soil moisture anomalies or slow soil moisture PC time series) is estimated as the ratio between the variance of the slow or predictable component and the variance of the total component, that is

$$p = \frac{V(\mu_y)}{V(x_{yo})} \tag{4}$$

It represents how large the seasonal mean variables can be potentially predicted (Madden 1976; Zheng and Frederiksen 1999).

3.3 Slow-PC (S-PC) prediction scheme

In Sect. 3.1, we have shown that the PC time series of the predictable soil moisture mode can be written as,

$$\mathbf{p}_y \equiv \mathbf{s}_{yo}^T \mathbf{V}. \tag{5}$$

where $\mathbf{s}_{yo}$ denote the seasonal mean soil moisture anomalies in year y, $\mathbf{V}$ denote the slow or predictable soil moisture EOF mode. Then,

$$\mathbf{s}_{yo}^T = \mathbf{p}_y \mathbf{V}^T. \tag{6}$$

As the EOF matrix $\mathbf{V}$ can be estimated using soil moisture data in a training period, the seasonal mean soil moisture field $\mathbf{s}_{yo}$ can be predicted given a prediction of $\mathbf{p}_y$.

3.4 Prediction skill

The skill score V_{exp}, expressed as the percentage of explained variance (Wilks 1995; Francis and Renwick 1998), is used for evaluation of our forecast scheme:

$$V_{\text{exp}} = 100\left(1 - \frac{1}{s}\right). \tag{7}$$

where,

$$s = \sum_i \sum_y \left[b_y(i) - o_y(i)\right]^2 \Big/ \sum_i \sum_y \left[p_y(i) - o_y(i)\right]^2, \tag{8}$$

Here, $o_y(i)$ is the CLM3.5/ObsFC simulated value of the seasonal mean soil moisture in year y and region i. $p_y(i)$ is the predicted values using S-PC prediction scheme, and $b_y(i)$ is the baseline forecast (usually climatology). The skill scores range from minus infinity to 1 (perfect forecast). Negative (/positive) values indicate that the forecast is less (/more) accurate than the climatology.

4 Predictable signals and their possible sources

4.1 Potential predictability of seasonal soil moisture in China

Our soil moisture seasonal forecasting analysis started with an initial estimation of the potential predictability (Sect. 3.2; Eq. 4) of the seasonal mean soil moisture in China, during the period 1951–2008. The potential predictability of the seasonal soil moisture (expressed as the ratio of slow to total variance; S/T) is quite high for the seasons from MAM to DJF (Table 1). This indicates that China's soil moisture is mainly associated with slow variability. An annual cycle in the potential predictability is obvious in Table 1; it is higher during cold seasons (SON and DJF) than warm seasons (MAM and JJA), with a maximum of 0.94 in winter (DJF). As the Eastern Asian summer monsoon develops, the potential predictability decreases, and reaches a minimum of 0.76 during summer (JJA).

The spatial distributions of the potential predictability of seasonal soil moisture in China during MAM–DJF are shown in Fig. 3. Consistent with the annual cycle of the potential predictability, as discussed above, in cold seasons (SON and DJF) it is significantly larger than in warm seasons (MAM and JJA) over most of mainland China. The potential predictability in all four seasons analyzed has a similar northwest–southeast gradient, with the highest levels of predictability mainly being located in the arid and semiarid areas of China. There are minimum centers over southeastern China; the region most influenced by the EAM. That a substantial component of interannual variability arises from intraseasonal variability over this area implies that there may be a connection between the intraseasonal variability of soil moisture and the intraseasonal variability of the EAM activity. This is in agreement with the study by Zuo and Zhang (2007), which suggests that high frequency of soil moisture variations over south China might relate to the variations of the EAM precipitation.

As the intraseasonal variance is responsible for the interannual variance of the soil moisture in China to a certain

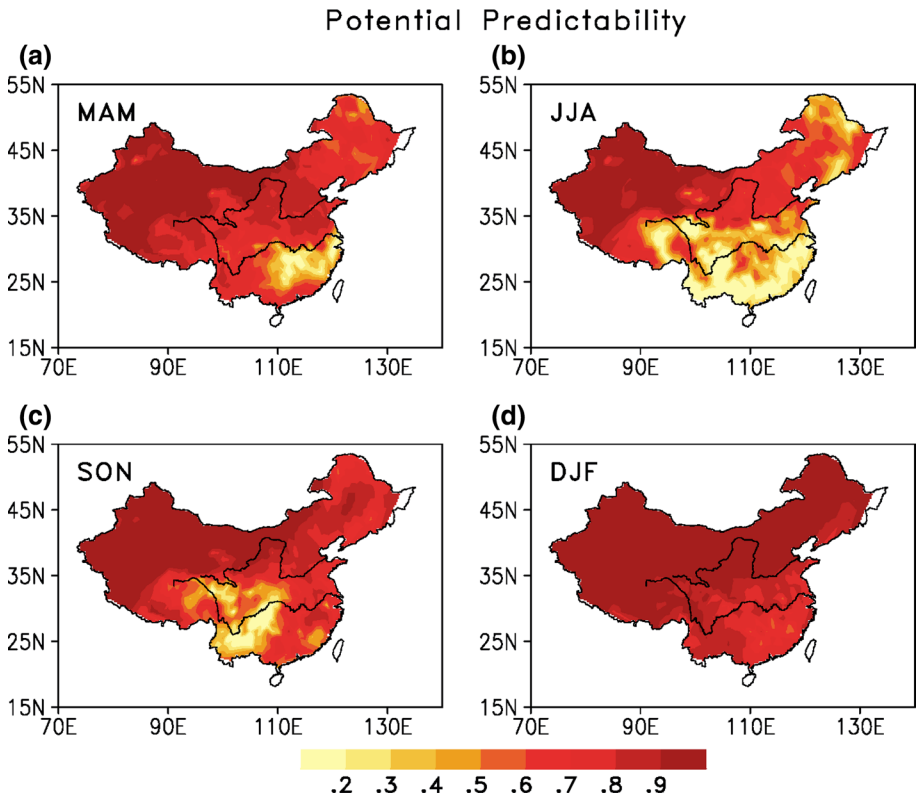

Fig. 3 Spatial distributions of the potential predictability of the top-1 m soil moisture across China during **a** MAM, **b** JJA, **c** SON and **d** DJF for the period 1951–2008

Table 2 The potential predictability of slow principal components (S-PCs) of top-1 m soil moisture in China for the period 1951–2008

Season	(% explained Var.) predictability					
	S-PC1	S-PC2	S-PC3	S-PC4	S-PC5	S-PC6
MAM	(22 %) 0.99	(16 %) 0.91	(9 %) 0.93	(7 %) 0.91	(5 %) 0.96	(4 %) 0.91
JJA	(20 %) 0.97	(14 %) 0.90	(8 %) 0.88	(6 %) 0.92	(5 %) 0.89	(5 %) 0.86
SON	(22 %) 0.99	(13 %) 0.96	(11 %) 0.97	(6 %) 0.84	(5 %) 0.93	(4 %) 0.96
DJF	(25 %) 1.00	(11 %) 0.98	(9 %) 0.94	(7 %) 0.83	(5 %) 0.97	(4 %) 0.92

The percentages of the variance explained are shown in brackets

extent, especially for the eastern part of China, it is important to separate the variance due to the intraseasonal component (noise) from the variance in the slow component (signal) in the construction of covariance matrix when focusing on the issue of seasonal predictability, by using the ZF2004 variance decomposition method. Then, by applying EOF analysis, we can derive the more predictable patterns of soil moisture in China. This allows us to focus on the more predictable signals of the seasonal mean, which we are most interested in. Table 2 provides a summary of the potential predictability of the leading six slow soil moisture modes in China for the seasons MAM–DJF, which explain more than 60 % of the variability in the slow component. The potential predictability of most of the soil moisture slow principal components (PCs) is more than 0.90; this comprises a larger predictability than the seasonal soil moisture PCs derived without the application of ZF2004 (values not shown). The six soil moisture slow PCs provide the majority of the skill of the predictive scheme (Sect. 5). Including other slow PCs added negligible additional skill, therefore we do not discuss them further.

4.2 Prediction skill from the soil moisture persistence

In the same way that the oceans can store heat and induce persistence ("memory") in the climate system, land represents a water storage for the climate system, with associated persistence features. In this section, by building a S-PC prediction scheme (Sect. 3.3), using soil moisture persistence as the only seasonal predictor, the importance of soil moisture memory for the seasonal forecasting of soil moisture in China is investigated. Here, the soil moisture persistence is represented by a projection of the one-season-lead soil moisture field onto the S-EOF matrix of

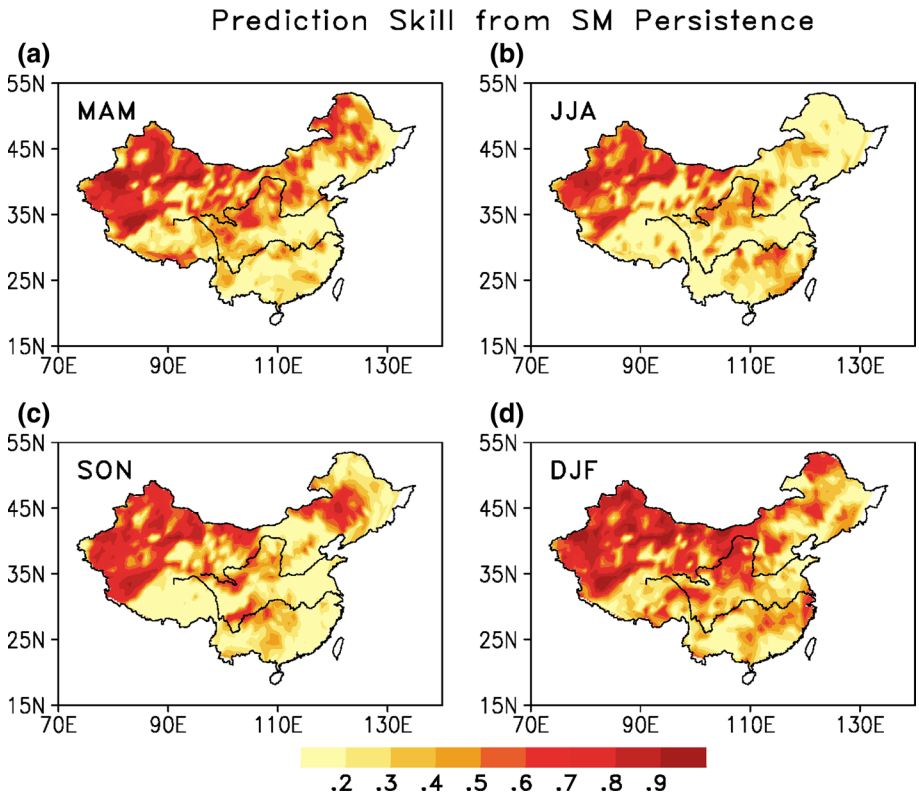

Fig. 4 Spatial distributions of the prediction skill for the top-1 m soil moisture across China during **a** MAM, **b** JJA, **c** SON and **d** DJF, using soil moisture persistence as the predictor. The training period of the prediction scheme was 1951–1991 and the verification period was 1992–2008

the soil moisture; for example, MAM soil moisture and JJA soil moisture S-EOF. Thus, similar to $\mathbf{p}_y$ (Eq. 5), it is denoted by $\mathbf{p}_{y1}$. As discussed in the previous section, the top six dominant slow soil moisture patterns during MAM–DJF explain a substantial amount of the interannual variability in the slow component and have considerable potential predictabilities. Therefore, we try to predict the leading six predictable soil moisture PCs using the soil moisture persistence, setting the other PCs to be zero. The period 1951–1991 is used as the training period and 1992–2008 is used as the verification period, for the predictive scheme. We estimate the connections between the PCs and the soil moisture persistence using linear regression during the training period. Then, the prediction skills (Eq. 7; Sect. 3.4) can be calculated during the verification period.

Figure 4 shows the spatial distributions of the prediction skill from soil moisture persistence. In general, the soil moisture persistence can produce considerable skillful forecasts, with the percentage explained variance of 51, 44, 52 and 65 % during MAM, JJA, SON and DJF, respectively. The predictive skill for the seasons MAM–DJF decreases similarly from the northwest to the southeast, consistent with the spatial distribution of the potential predictability (Fig. 3). The average prediction skill is more than 50 % of the average potential predictability, indicating the previous soil moisture conditions is the dominant predictor for seasonal soil moisture predictions in China. However, there is still some soil moisture variance cannot be predicted from previous soil moisture. This indicates that the sources of predictability for the soil moisture in China may originate from the contemporary conditions of the atmospheric variables, such as precipitation, temperature and wind speed, in addition to the lagged soil moisture conditions. Climate predictors (e.g. the SSTs and the linear trend, among others) can be used to predict the simultaneous atmospheric circulation conditions in China. Therefore, we examine the role of these possible predictors on the seasonal soil moisture over China in the following sections.

4.3 Predictable modes with their possible predictors of SST and linear trend

In this section, the slow soil moisture modes with long-term trends are identified. Possible sources of predictability from SSTs are also investigated by constructing lead-lag correlation maps (e.g. the SSTs of MAM and the soil moisture of JJA). The data period used for this section is from 1951 to 1991, which corresponds to the training period for the forecast scheme. To aid the physical interpretation of the slow modes, we examine the atmospheric circulations associated with the predictable soil moisture modes; this is done by estimating the covariance between the standardized soil moisture slow PC time series and the standardized circulation variable's time series, using Eq. (3). The slow

covariance patterns are associated with very slowly varying (interannual to supra-annual) external forcings and internal dynamics (Frederiksen and Zheng 2004), which help us to understand the sources of predictability for seasonal soil moisture from atmospheric circulations.

It should be noted that, since the soil moisture effectively integrates the time history of the circulation factors (such as temperature, rainfall and wind speed), the lagged effects can be as important as those that are contemporaneous with the soil moisture. Consequently, both the concurrent and lead-lag relationships between the predictable soil moisture signals and the precipitation, temperature and wind speed fields have been examined. However, we only show the covariance maps with the maximum covariance values in this paper. In particular, the covariances between the 1-month-lead seasonal precipitation/temperature/wind fields, and the slow soil moisture modes are shown for MAM, JJA and SON (e.g. the precipitation, temperature and wind speed fields of FMA and the soil moisture slow PCs of MAM). In addition, the covariances between the soil moisture slow PCs and the 1-season-lead precipitation, temperature and wind speed fields are shown for DJF, i.e., the soil moisture at winter freeze-up is greatly affected by the fall (SON) precipitation, temperature and wind speed conditions.

4.3.1 *Predictable soil moisture mode related to the Indian Ocean SST*

The second MAM slow soil moisture mode (16 % explained variance), and its associated SST and circulation factors are shown in Fig. 5. During the phase shown in Fig. 5, the second MAM slow soil moisture mode has positive anomalies (Fig. 5a), corresponding to the wet conditions over north central China. Associated with this phase of the mode, there is an increase in rainfall, and decrease in temperature and wind speed, over north central China (Fig. 5e–g).

Remarkable features that appear in the one-season-lead SST correlation pattern are the maximum center values in the Indian Ocean (Fig. 5c). These indicate that the MAM second slow mode is associated with significant warming in the Indian Ocean. The slow covariance of 500-hPa geopotential height associated with the MAM S-EOF2 (Fig. 5d) displays a spatial pattern in the extra tropical region that is similar to the Slow-REOF3, in Figure 4 of Frederiksen and Zheng (2004), identified to be the Western Pacific Oscillation (WPO) and significantly related to the Indian and eastern tropical Pacific SSTs. Over the low- and mid-latitude areas, there is a strong positive center close to the Philippine Sea, which is the area most affected by the western Pacific subtropical high (WPSH); this indicates that the WPSH may also be an important factor that affects soil moisture in China. This is consistent with the study by He and Zhou (2015), where the relationship between the tropical Indian Ocean SSTs and the WPSH was described; their study indicated that a stronger warming in the tropical Indian Ocean is associated with an enhanced WPSH, which further increases the precipitation over the northern part of eastern China, with an enhanced southerly wind.

4.3.2 *Predictable soil moisture mode related to the North Atlantic and Kuroshio SSTs*

Figure 6 shows the leading predictable soil moisture pattern and its associated PC time series during JJA, and its associated SST and circulation patterns. The explained variance of this mode is 20 %. At the phase shown here, it is positive loadings that correspond to the wet conditions over northwestern China (Fig. 6a). This can be explained by the wetter than normal precipitation, cooler than normal temperature and lower than normal wind speed conditions in the northwest of China (Fig. 6e–g).

During the period 1951–1991, significant prolonged positive trends can be observed in the time series of this predictable soil moisture mode (Fig. 6b). Therefore, we examine the relationship between the detrended JJA S-PC1 and the detrended global SSTs (Fig. 6c). That is, the linear trend is removed from both the time series of the JJA leading slow mode and the SSTs on each grid. The one-point correlation map of the one-season-lead SSTs shows that the North Atlantic is significantly cooler in the north and warmer in the south; this indicates a strong teleconnection between the soil moisture in China and the North Atlantic tripole SST variability. The covariance of the 500 hPa geopotential height (Fig. 6d) associated with the JJA leading slow mode shows a Northern Annular Mode (NAM)-like zonal structure [see S-REOF1 of Frederiksen and Zheng (2004)] over the North Atlantic Ocean. This consists of a dipole structure, with centers of opposite signs over Greenland and Northern Europe, and is closely connected with the Northern Atlantic SSTs. Previous studies have revealed a close relationship between the North Atlantic SST anomalies and the interannual variations of China's temperature (Wu et al. 2011), the EAM (Zuo et al. 2012, 2013) and the EAM rainfall (Gu et al. 2009), through air-sea interactions over the Atlantic-Eurasia region.

Another notable feature in the one-point SST correlations with the JJA leading predictable mode, is the significantly warmer SSTs over the northwestern Pacific Ocean around the Kuroshio region, and the Indian Ocean during this phase; this indicates a close relationship between the soil moisture in China and the variability in SSTs in these areas. An anti-cyclonic anomalies center of the 500 hPa geopotential height covariance pattern is mainly located from the west side of the Philippines to the east coastline

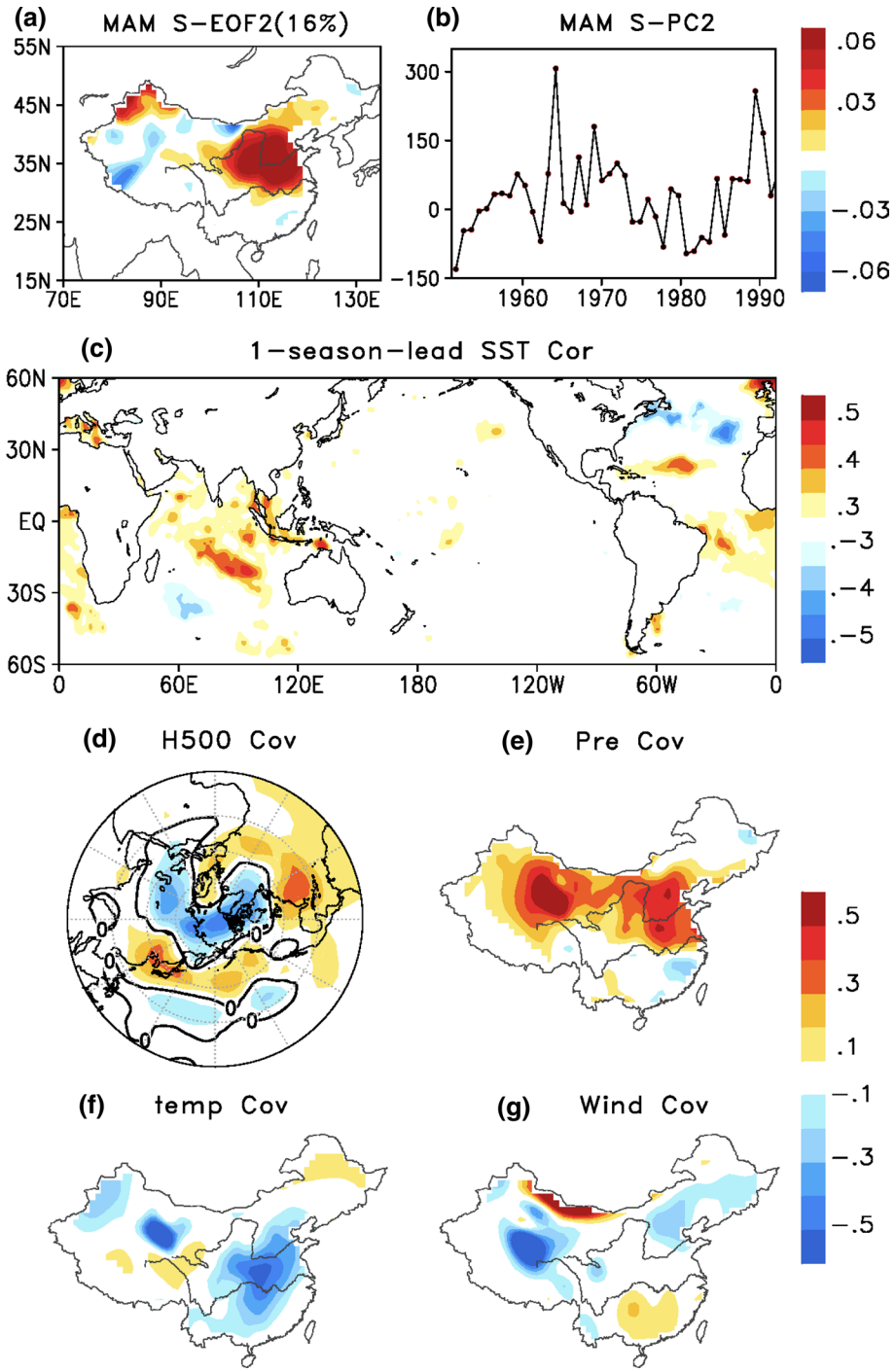

Fig. 5 The **a** spatial and **b** temporal patterns of the second MAM slow soil moisture mode in the top-1 m soil layer across China (explained variance in *bracket*) and **c** the 1-season lead-lag correlation between the associated time series for the slow mode and the SSTs, and the covariances between the PC time series for the slow mode and the slow component of the **d** contemporary 500 hPa geopotential height, **e** precipitation, **f** temperature and **g** 2 m wind speed, for the training period 1951–1991

of Africa, at latitudes between 10°N and 30°N. This is the area most influenced by the WPSH, indicating that it may be an important factor that affects soil moisture in China during JJA. This is consistent with our previous study (Ying et al. 2013), in which we found a significant relationship between the interannual variability of the Kuroshio SSTs and summer rainfall in eastern China, by linking the intensity and position of the WPSH.

4.3.3 Predictable soil moisture modes related to ENSO

The top two rows of Fig. 7 show the second predictable soil moisture modes and their associated PC time series during SON and DJF, which explained 13 and 11 % of the variance, respectively. There are similar spatial structures in the loadings of these two soil moisture modes. During this phase, it is drier than normal in the north central China and

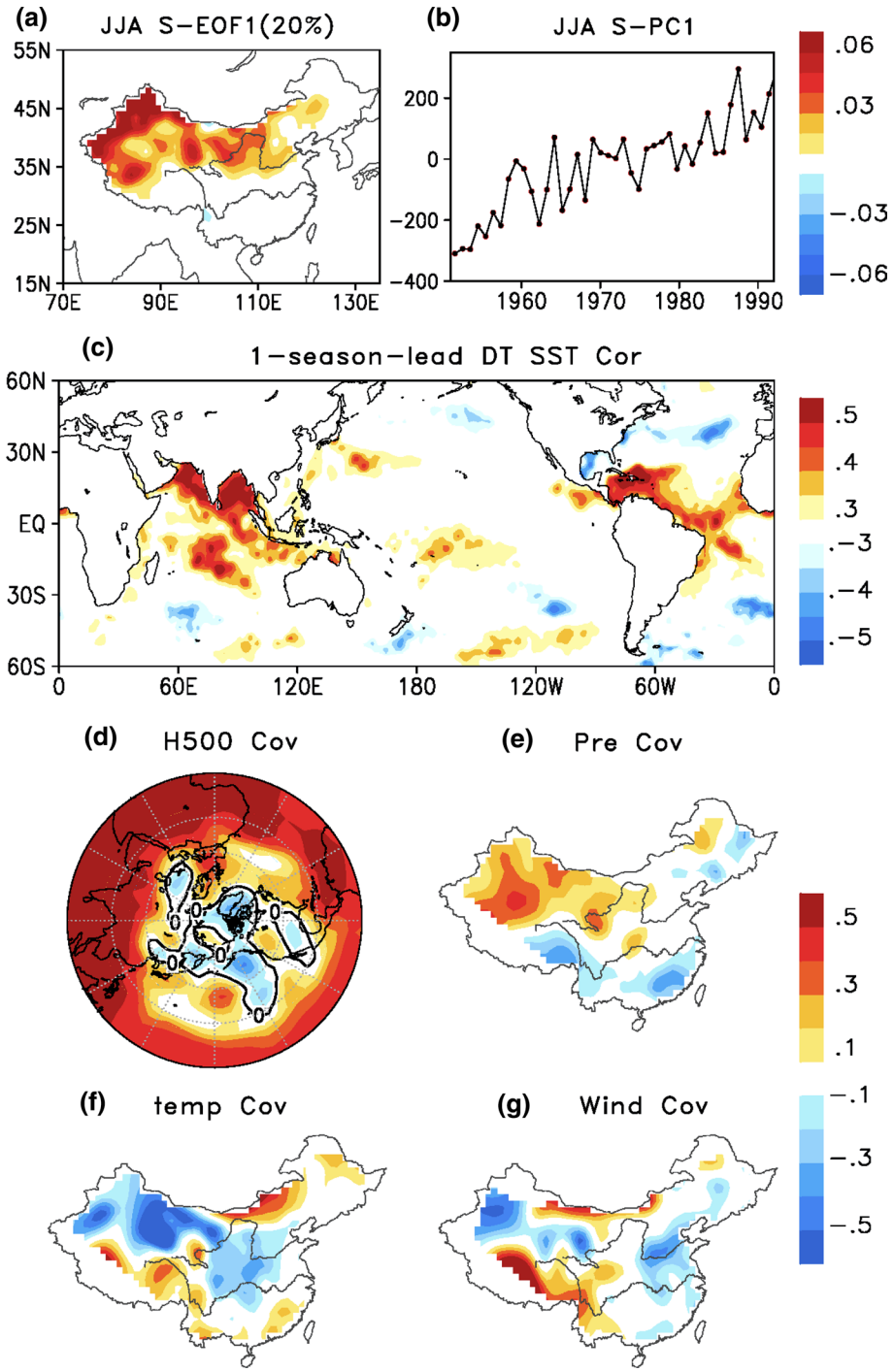

Fig. 6 The **a** spatial and **b** temporal patterns of the leading JJA slow soil moisture mode in the top-1 m soil layer across China (explained variance in *bracket*) and **c** the 1-season lead-lag correlation between the detrended associated time series for the slow mode and the detrended SSTs, and the covariances between the PC time series for the slow mode and the slow component of the **d** contemporary 500 hPa geopotential height, **e** precipitation, **f** temperature and **g** 2 m wind speed, for the training period 1951–1991

wetter than normal in the rest of China. The covariances between these two modes and the circulation factors reveal that the second soil moisture slow modes during SON and DJF are dominated by the precipitation conditions over China (Fig. 7e, l). In particular, the precipitation has negative anomalies in north central China and positive anomalies in the rest of China, resulting in the corresponding soil moisture conditions over China.

The one-season-lead SST correlations associated with the second slow soil moisture modes during the seasons SON and DJF (Fig. 7c, j) indicate that these two modes are associated with significant warming over the eastern tropical Pacific Ocean, which suggests the impact of El Niño/Southern Oscillation (ENSO) on soil moisture variability. From Fig. 7d, k, the covariance patterns of the 500 hPa geopotential height associated with the second slow soil

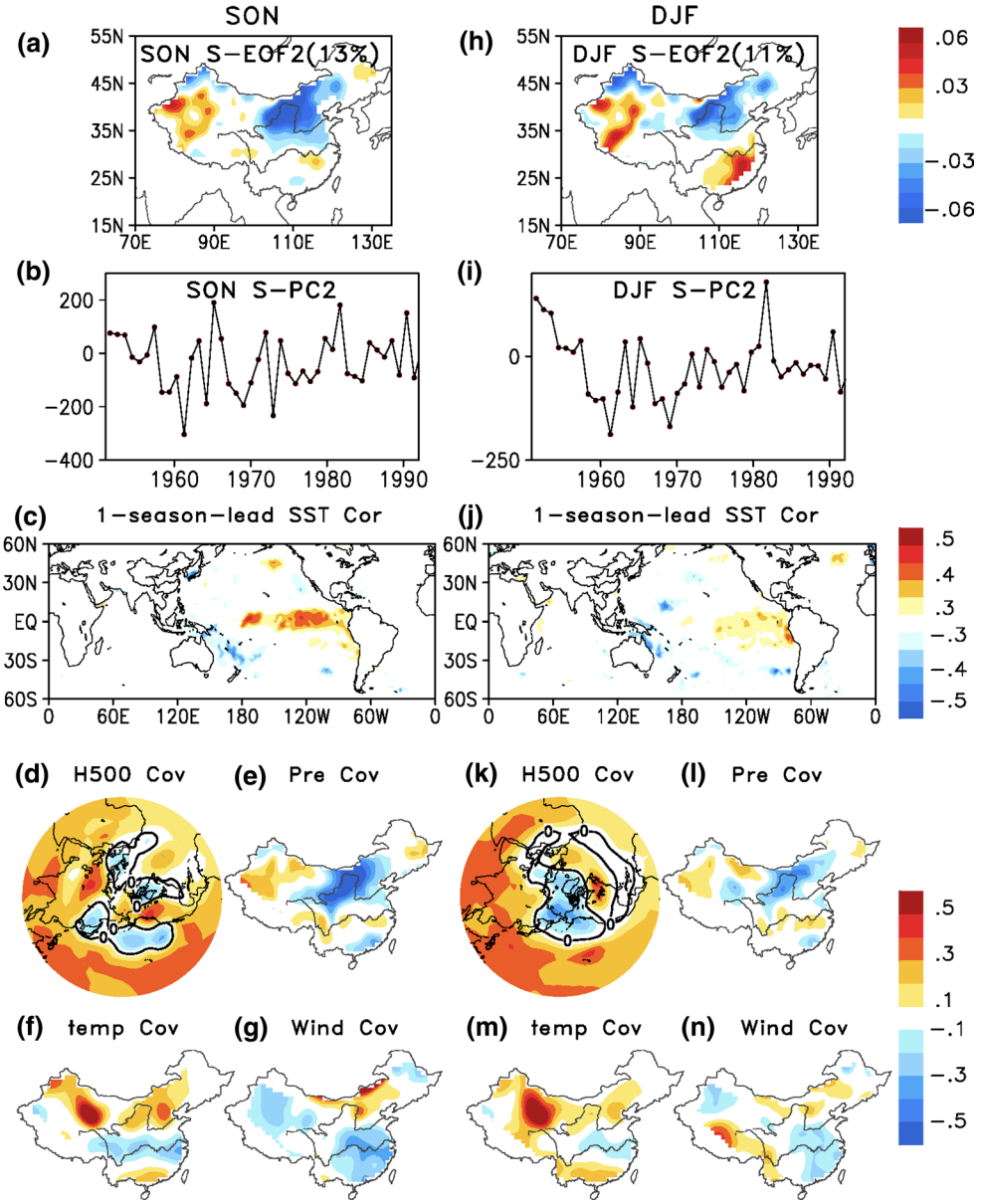

Fig. 7 **a**–**g** and **h**–**n** shows the same as in Fig. 5, but for the second slow soil moisture modes of SON (*left panel*) and DJF (*right panel*), respectively

moisture modes during SON and DJF all show a Pacific North American (PNA)-like pattern over North America, as described in Frederiksen and Zheng (2004; slow-REOF2), which was found to be highly related to ENSO. Besides the large scale PNA circulation pattern, the 500 hPa height covariance distribution shows that the predictable soil moisture variability in China is also driven by the WPSH, as there is a significant positive center situated over the area that is mostly influenced by the WPSH. This is consistent with various studies that have investigated the connections between the interannual variability of the East Asia climate and ENSO (e.g. Huang and Sun 1994; Liu and Ding 1995; Chang et al. 2000; Gong and Ho 2002; Wang et al. 2000, Wang and Li 2004; Zhou et al. 2008, 2011, 2013). These studies concluded that the WPSH and PNA teleconnections (Zhang et al. 1999; Wu et al. 2003; Zhou et al. 2009; Ying et al. 2013, 2015) are one of the major factors that control the interactions of the two dynamic systems over this region.

4.3.4 Predictable soil moisture modes with long-term trend

Trends in climate data are, of course, a source of predictability. From the discussions above, we have found that the PC time series associated with the JJA leading predictable modes of China soil moisture exhibit a significant linear trend during the period of 1951–1991, as shown in Fig. 6b. Actually, for the leading slow modes of MAM, SON and DJF, their associated PC time series also show a significant prolonged trends from 1951 to 1991. The spatial and temporal patterns of these slow soil moisture modes are

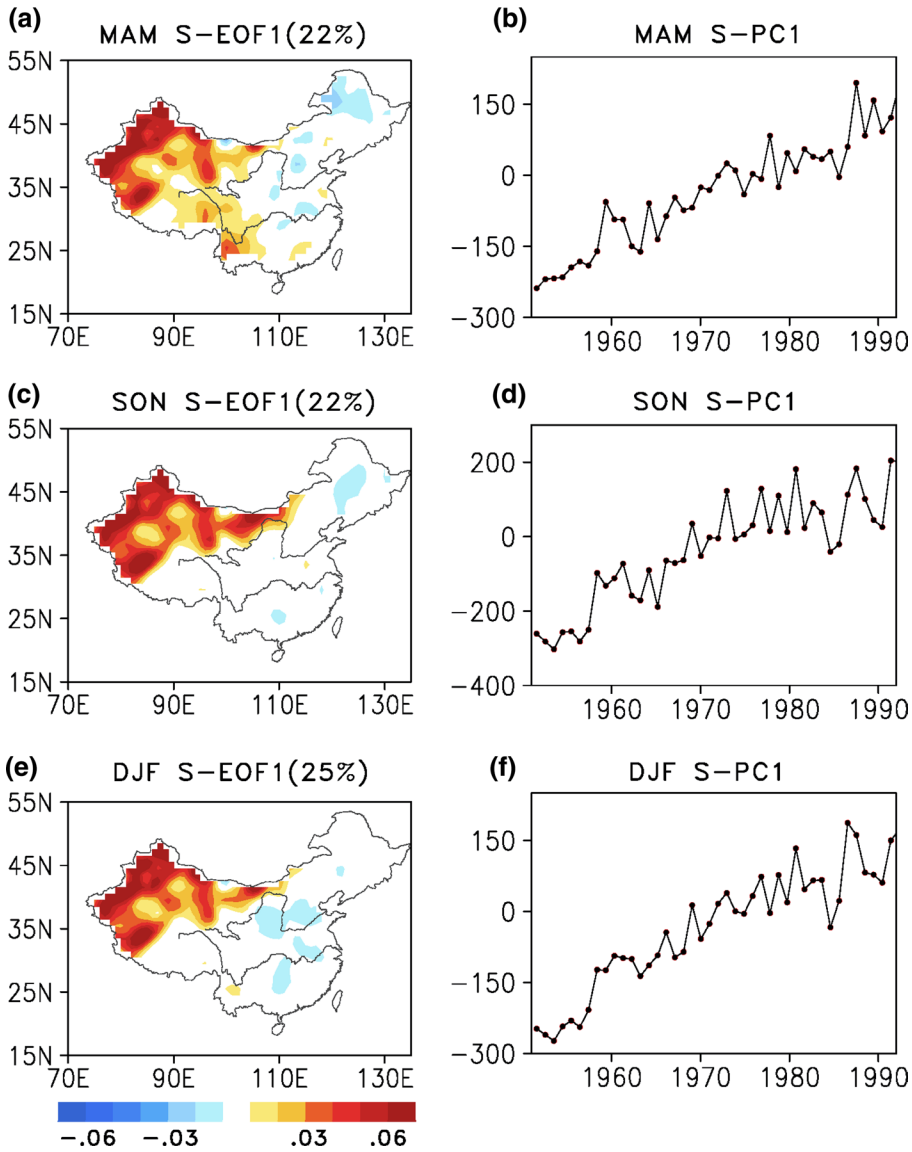

Fig. 8 **a–b**, **c–d** and **e–f** shows the same as in Fig. 5a–b, but for the leading slow soil moisture modes of MAM (*top*), SON (*middle*) and DJF (*bottom*), respectively

shown in Fig. 8. It can be seen that a steep wetting trend occurred over northwestern China, including Xinjiang, most of the Tibetan Plateau and the western part of Inner Mongolia for all the four seasons MAM–DJF. This is generally consistent with the previous study by Wang et al. (2011) that found the soil moisture in most of Xinjiang, the Tibetan Plateau and small areas over south China has significant upward trends during the period of 1950–2006; in their study, four different land surface hydrology models driven by Princeton's meteorological dataset (Sheffield et al. 2006) were used to simulate the soil moisture over China. However, we give a further consideration of the seasonality. Based on in situ observations, Wang and Zhou (2005) and Chen et al. (2014) analyzed the trends in the annual, seasonal mean and extreme precipitation in China during the last 50 years. They concluded that there were increasing trends across most of northwest China in all seasons. Li et al. (2015) further explored the reason why the precipitation in northwest China shows a significant increasing trend since the 1960s based on the monthly precipitation from 74 weather stations in northwest China, and suggested that the strengthening of the WPSH and the North American Subtropical High after the mid-1980s was probably the main cause. As soil moisture is largely related to precipitation, these findings are consistent with our study and may explain the soil moisture trends we have observed. Besides the observed wetting trend of precipitation, previous studies also found that there is an increase in glacial melt water, river runoff and water level of inland lakes, and an improved vegetation cover during the last decades in the northwestern China (Shi et al. 2007; Xu et al. 2007; Zhang et al. 2003); and they concluded that this is a consequence of global warming and an enhanced water cycle.

Table 3 Predictors of slow principal components (S-PCs) of top-1 m soil moisture in China that are selected from the training period 1951–1991

Season	Predictors		
	S-PC1	S-PC2	S-PC3 ~ 6
MAM	$\mathbf{P}_{y1}$***, trend*	$\mathbf{P}_{y1}$***, Feb Indian SST*	$\mathbf{P}_{y1}$
JJA	$\mathbf{P}_{y1}$***, May Atlantic SST*	$\mathbf{P}_{y1}$***	$\mathbf{P}_{y1}$
SON	$\mathbf{P}_{y1}$***	$\mathbf{P}_{y1}$***, JJA Niño-4 SST*	$\mathbf{P}_{y1}$
DJF	trend***, $\mathbf{P}_{y1}$***	$\mathbf{P}_{y1}$***	$\mathbf{P}_{y1}$

* 0.05, *** 0.001

5 Prediction scheme

In this section, we try to construct a S-PC prediction scheme, similar to that in Sect. 4.2, but using the predictors form the soil moisture persistence as well as a set of possible predictors identified in the Sect. 4.3. The predictors that are most appropriate to train the regression coefficients are selected using a stepwise regression. For flexibility, we calculate the X(X = 1, 2, 3)-month(s)-lead values of the possible predictors; for example, the SSTs of March, April, May and MAM and the soil moisture of JJA. The results are listed in Table 3. The selected predictors are all above 95 % significant.

The leading MAM predictable soil moisture mode has a long-term trend in the associated PC time series (Sect. 4.3.4). So we choose the prolonged trends and soil moisture persistence as the possible predictors. The analysis shows that both of them are chosen to be the best predictors for this mode. As we have shown in Sect. 4.3.1, the second slow soil moisture mode in MAM is clearly associated with the SST anomalies in Indian Ocean (70°–100°E, 20°S–15°N). Therefore, we consider the lagged Indian SST and soil moisture persistence as candidate predictors of the soil moisture MAM S-PC2. In this case, the stepwise regression selected the soil moisture persistence and the February Indian SST as the best predictors.

For the first slow soil moisture mode in JJA, significant linear trend can be seen in the associated PC time series, and it is closely associated with the interannual variability of SSTs over the Indian Ocean, Kuroshio (130°–150°E, 20°–40°N) and Atlantic Ocean (where there is a difference between the north (40°–55°N, 60°–40°W) and south (25°–35°N, 80°–60°W), as discussed in Sect. 4.3.2. Taking the lagged SSTs (over the specific areas mentioned above), the trend and the soil moisture persistence into the stepwise regression equation, the soil moisture persistence and May Atlantic tripole have been selected as the best predictors. Neither the linear trend, nor the Indian Ocean or Kuroshio SSTs were selected as predictors, presumably owing to the fact that they are significantly correlated to the previous soil moisture conditions.

During SON and DJF, the leading predictable soil moisture modes display a significant linear trend in the associated PC time series (Sect. 4.3.4), while the second slow soil moisture modes are highly related to the tropical eastern Pacific (TEP) SSTs (Sect. 4.3.3). Therefore, the linear trends and soil moisture persistence are considered as possible predictors for the first slow modes. The lagged SSTs over the TEP (5°S–5°N, 70°–180°W), Niño-3 (5°S–5°N, 150°–90°W), Niño-4 (5°S–5°N, 160°E–150°W), Niño-3.4 (5°S–5°N, 170°–120°W) and Niño-1 + 2 (0°–10°S, 90°–80°W), at 1–3 month(s) lead or one-season-lead, as well as the soil moisture persistence, are considered as possible predictors for the second slow modes. The analysis shows that the soil moisture persistence is the best predictor for the leading slow mode during SON, and both the linear trend and the soil moisture persistence are the best predictors for the leading slow mode of DJF. For SON S-PC2, the best predictors are the JJA Niño-4 SST and the soil moisture persistence. Presumably due to the close relationship between ENSO SST and previous soil moisture conditions, soil moisture persistence rather than ENSO SST is the best predictor for DJF S-PC2.

For the rest of the predictable modes, there are no significant linear trends in their associated PC time series and they are not significantly correlated with the lagged SSTs. However, all of them could be predicted well using the soil moisture persistence. So the soil moisture persistence is used as the predictor. Note, we only predict the leading six soil moisture slow PCs. We have also tried to predict other predictable soil moisture modes, but found that they add negligible additional prediction skills, due to their limited explained variances and potential predictabilities. Therefore, these are set to zero.

Generally speaking, using the estimated PC relationships in Table 3, the prediction skills of soil moisture in China reach 59, 51, 62 and 77 %, from MAM to DJF, respectively. The spatial distributions of the prediction skills during MAM–DJF are shown in Fig. 9. The prediction skills are relatively lower than the theoretical estimates of the predictability (Fig. 3; Sect. 4.1), as expected. Compared to the prediction skill using only soil moisture persistence (Fig. 4; Sect. 4.2), better prediction skills are achieved over most of China, for all four seasons. This indicates that the prediction skill in China comes from the climate predictors such as the lagged SSTs and linear trends, as well as the soil moisture persistence.

The spatial distributions of the climatology mean and total variance of the predicted seasonal top-1 m soil moisture in China, during the verification period (1992–2008)

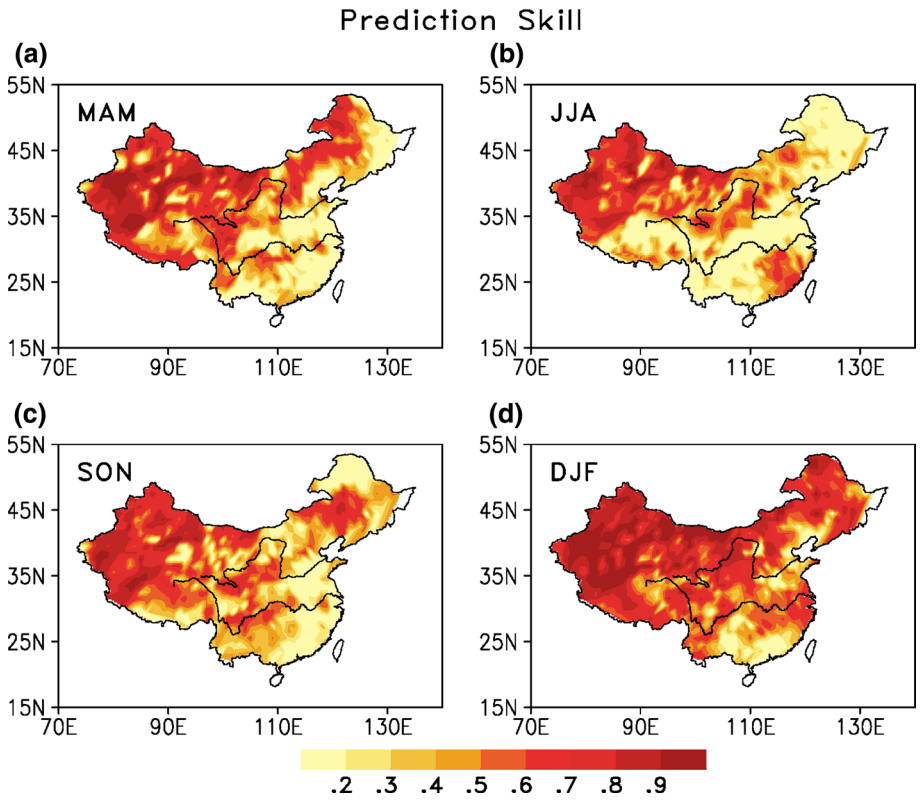

Fig. 9 Same as Fig. 4, but using the predictors described in Table 3

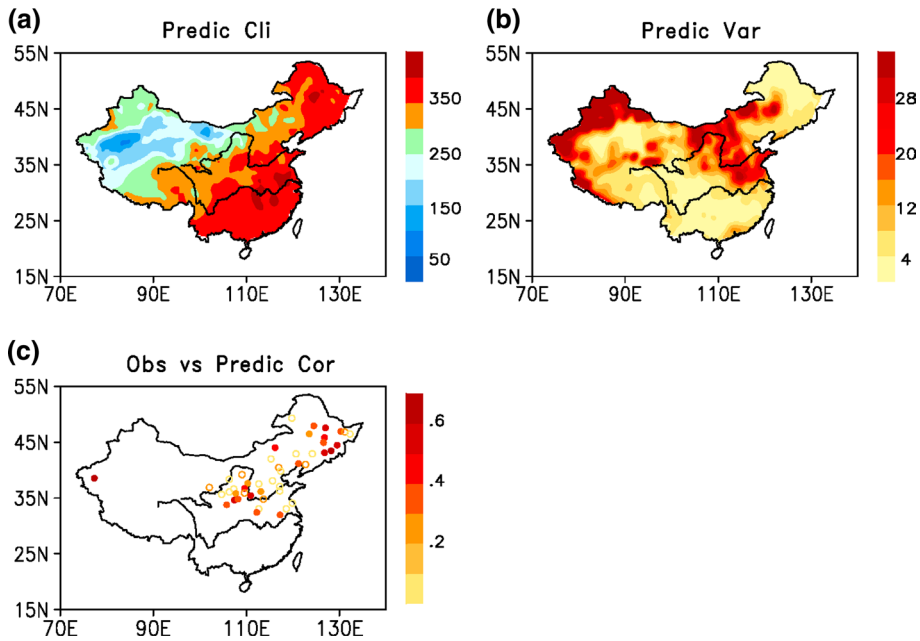

Fig. 10 Spatial distribution of the **a** climatology means and **b** variances for the S-PC scheme predicted top-1 m soil moisture; and **c** the correlation between the seasonal mean soil moisture observations and predictions, during the period 1992–2008 (MAM, JJA and SON). *Solid cycles* indicate correlation coefficients significant above 95 % confidence level according to the Student *t* test

are shown in Fig. 10a, b. Compared with Fig. 2i, j, there are quite similar spatial structures between the CLM3.5/ObsFC simulations and predictions, and they also generally capture the observed characteristics of the soil moisture (Fig. 2f, g). The correlations between the predicted seasonal soil moisture and the in situ observations are also shown in Fig. 10c. The spatial mean of the correlations is about 0.3 across China; this indicates that the prediction scheme has some practical applicability for seasonal forecasting of soil moisture anomalies in China.

We also use a simple grid prediction approach, with a stepwise regression to select the predictors from the

potential climate predictors (such as, previous soil moisture, SSTs in the Indian Ocean, Kuroshio, North Atlantic and TEP, linear trends and climate indices) for each individual grid. However, the prediction skills are 0.39, 0.23, 0.49 and 0.67 for the four seasons from MAM to DJF, respectively. The average correlation between the simple grid scheme predictions and the in situ observations is only 0.12. In this case, the total soil moisture without variance decomposition has been used. However, as we have discussed, a substantial component of the interannual variability in soil moisture across China arises from the intraseasonal (or unpredictable) component, especially during the warm seasons (MAM and JJA), and in the regions influenced by the EAM. As a result, without the decomposition, the intraseasonal component of soil moisture variability plays a role in reducing the predictability. In our methods, we focus on the leading EOFs of the slow component, which are potentially predictable; therefore, we avoid this problem.

6 Unpredictable modes

The principal aim of our research is to identify the most potentially predictable signals for the seasonal forecasting of soil moisture in China. However, as discussed in Sect. 4.1, the interannual variability of soil moisture in China is also related, to a certain extent, to the intraseasonal

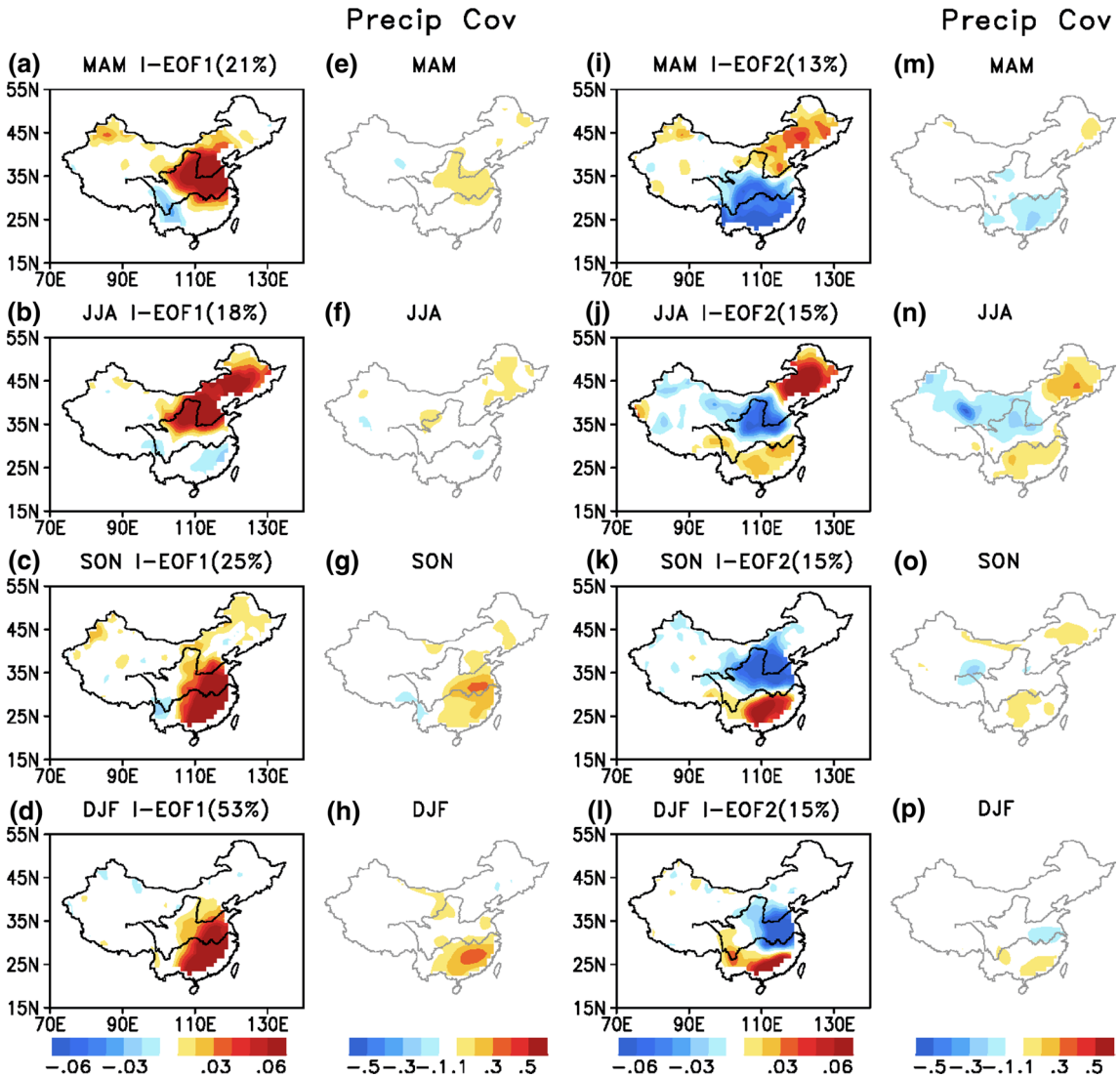

Fig. 11 Spatial patterns of the **a–d** first and **i–l** second intraseasonal soil moisture modes in the top-1 m soil layer across China; and **e–h** and **m–p** the covariance between the associated time series of the intraseasonal soil moisture modes and the intraseasonal component of contemporary rainfall, for the period 1951–2008

component, especially in eastern China. Therefore, it is also worthwhile to investigate the sources of uncertainty in prediction of the seasonal soil moisture. In this section, we consider the intraseasonal modes of interannual variability, by applying an EOF analysis to the intraseasonal variance matrix. Furthermore, we examine the associated atmospheric forcings; done to aid the physical interpretation of these intraseasonal soil moisture modes, by estimating the covariance between the PC time series of the intraseasonal soil moisture EOFs and the intraseasonal component of the atmospheric forcing fields.

Figure 11a–d, i–l shows the first two intraseasonal soil moisture modes from MAM to DJF. Unlike the predictable soil moisture modes, which are controlled by a complex combination of precipitation, temperature and wind speed, the leading two intraseasonal modes are not significantly correlated with temperature or wind speed (figures not shown). They are dominated by the contemporary precipitation, as shown in Fig. 11e–h, m–p. The most notable features of the intraseasonal EOF1s during MAM–DJF are the localized structures over eastern China. In particular, there are positive anomalies, corresponding to wetter-than-normal

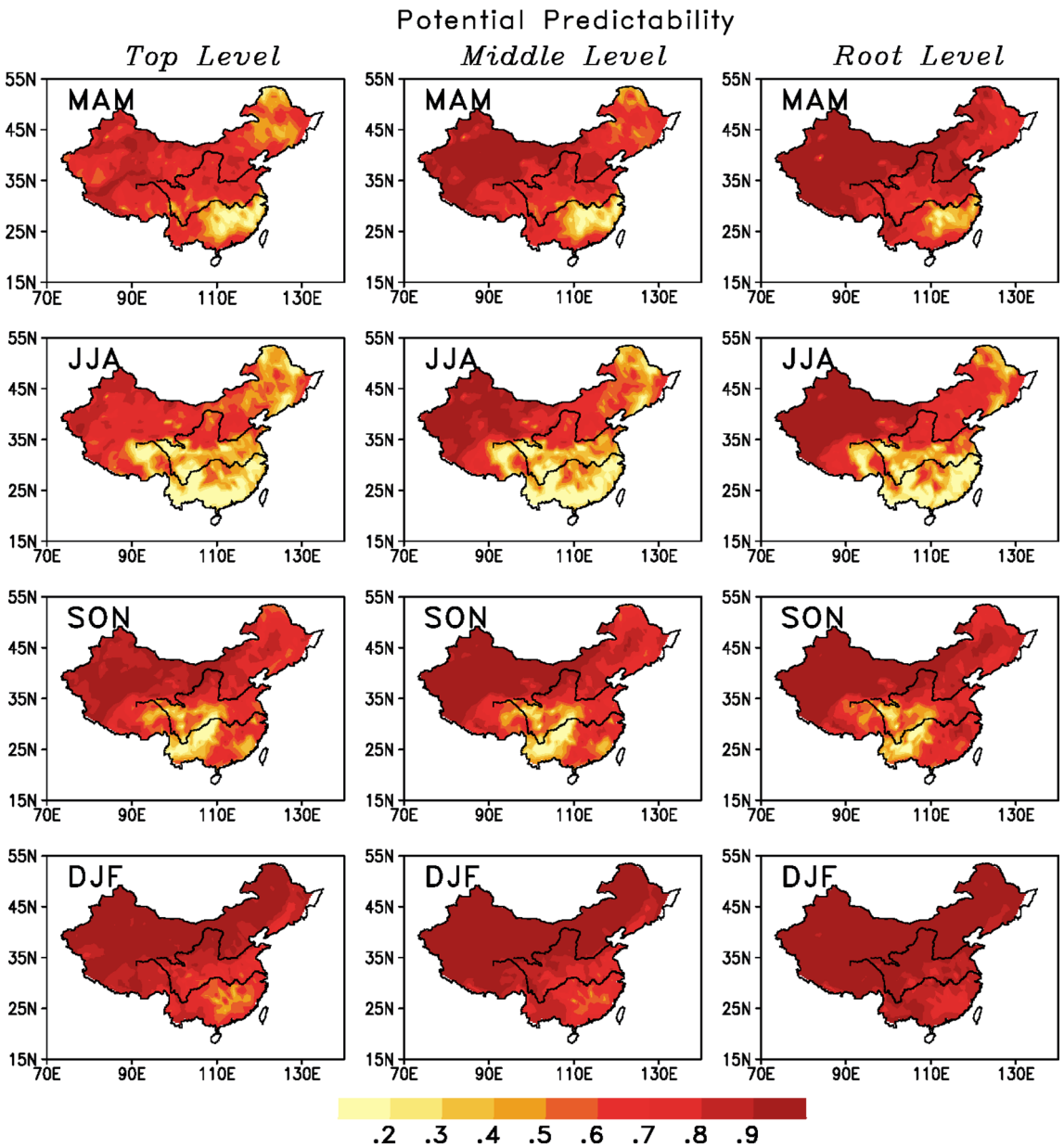

Fig. 12 The spatial distribution of the potential predictability of the soil moisture in the top (0.062 m; *left column*), middle (0.366 m; *middle column*) and root (1.040 m; *right column*) levels, across China for the period 1951–2008

soil moisture conditions, over the central and northern parts of eastern China during MAM and JJA, and over southeastern China during SON and DJF. Note that the centers of maximum amplitude for the leading intraseasonal modes are located in the areas mostly influenced by the EAM. This is consistent with the results in Sect. 4.1 and indicates that a substantial component of interannual variability arises from intraseasonal variability over this region.

Although the intraseasonal patterns are unpredictable at long ranges (a season or more ahead), they could be predictable from the beginning of the season, especially for their lifetimes in the first month of the season (Shukla 1983). It would be possible to improve the seasonal prediction skill if it were the case. The present analysis has suggested that EAM activity and the precipitation patterns should be highlighted for improving dynamical seasonal

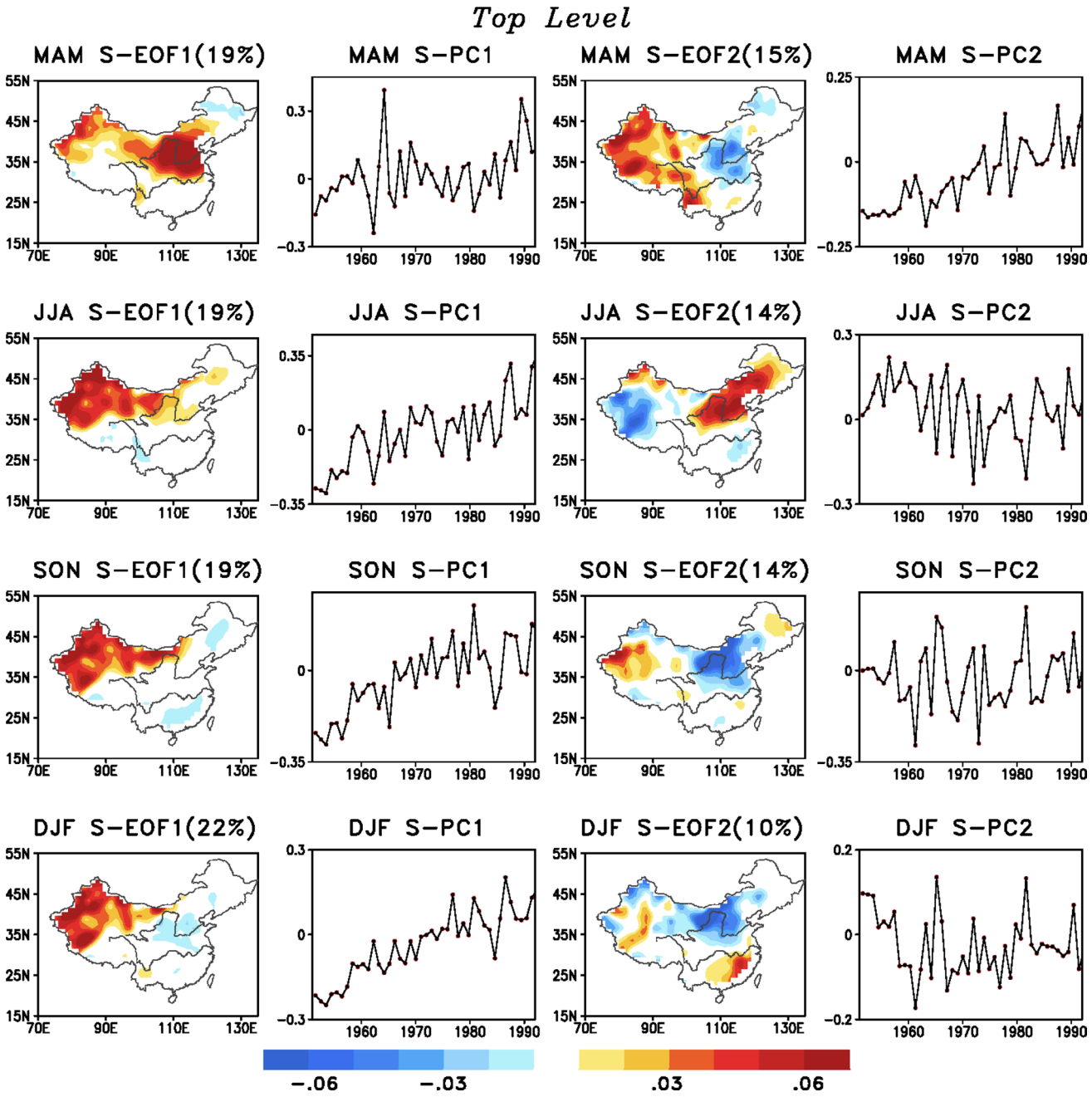

Fig. 13 Spatial and temporal patterns of the leading (*left two columns*) and the second (*right two columns*) slow soil moisture modes of the top (0.062 m) level (explained variance in *bracket*) from MAM to DJF for the period 1951–1991

forecasting from the beginning of the season, which influence the dominant modes of intraseasonal variability.

7 Conclusions and discussions

Observation-based meteorological data were used to force the land surface model CLM3.5 to simulate soil moisture over China for the period 1951–2008. The method of ZF2004 was then applied to the simulated soil moisture in China for the four seasons of MAM, JJA, SON and DJF, respectively, to decompose the total interannual variances of each season into the variance of a slow and more predictable component, and the variance of a noisier component associated with intraseasonal variability. Using the ratio of the variance of the predictable signal to the variance of the total seasonal mean anomalies as a preliminary estimation of the potential predictability, the annual

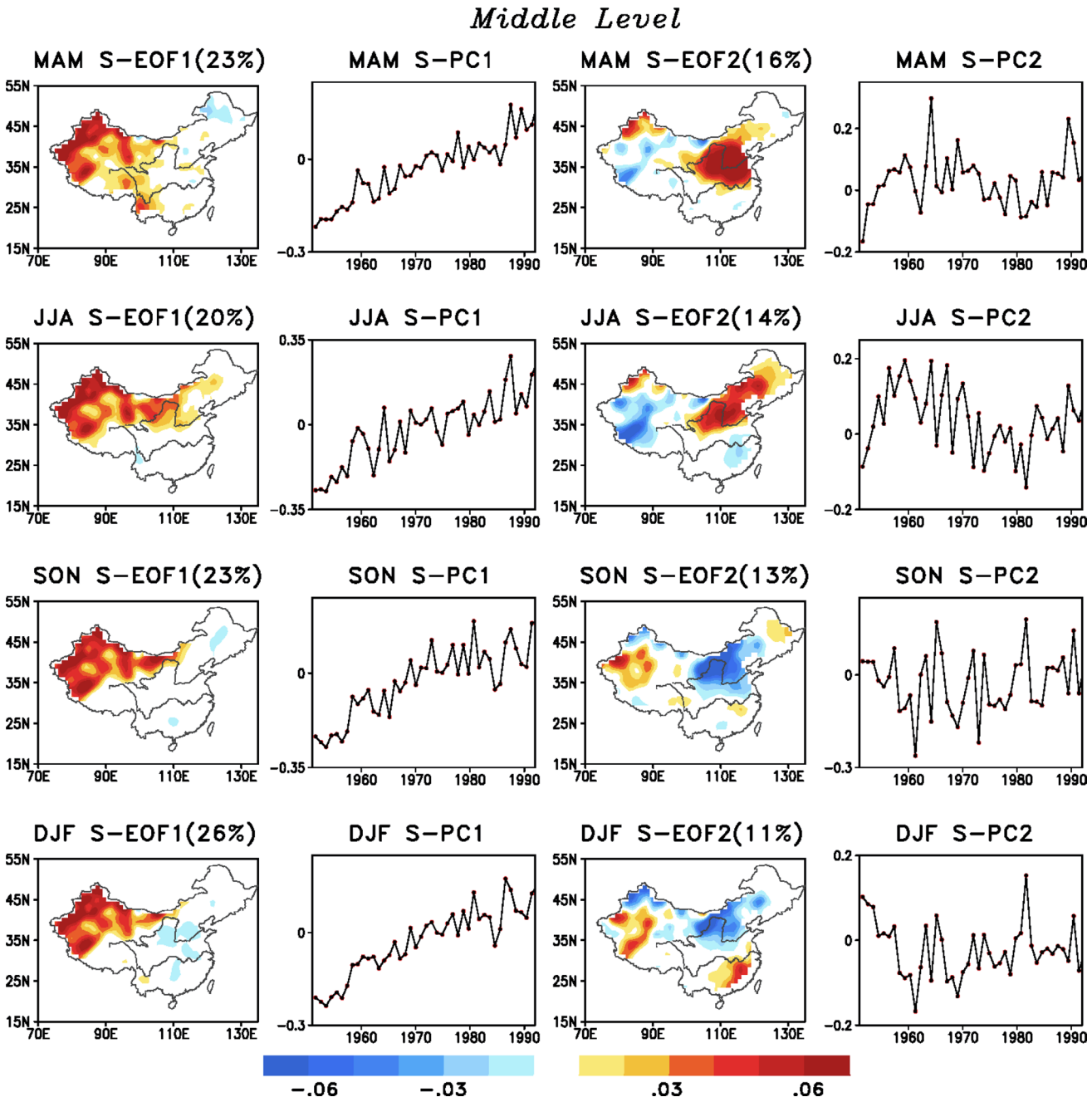

Fig. 14 Same as Fig. 13, but for the middle (0.366 m) level

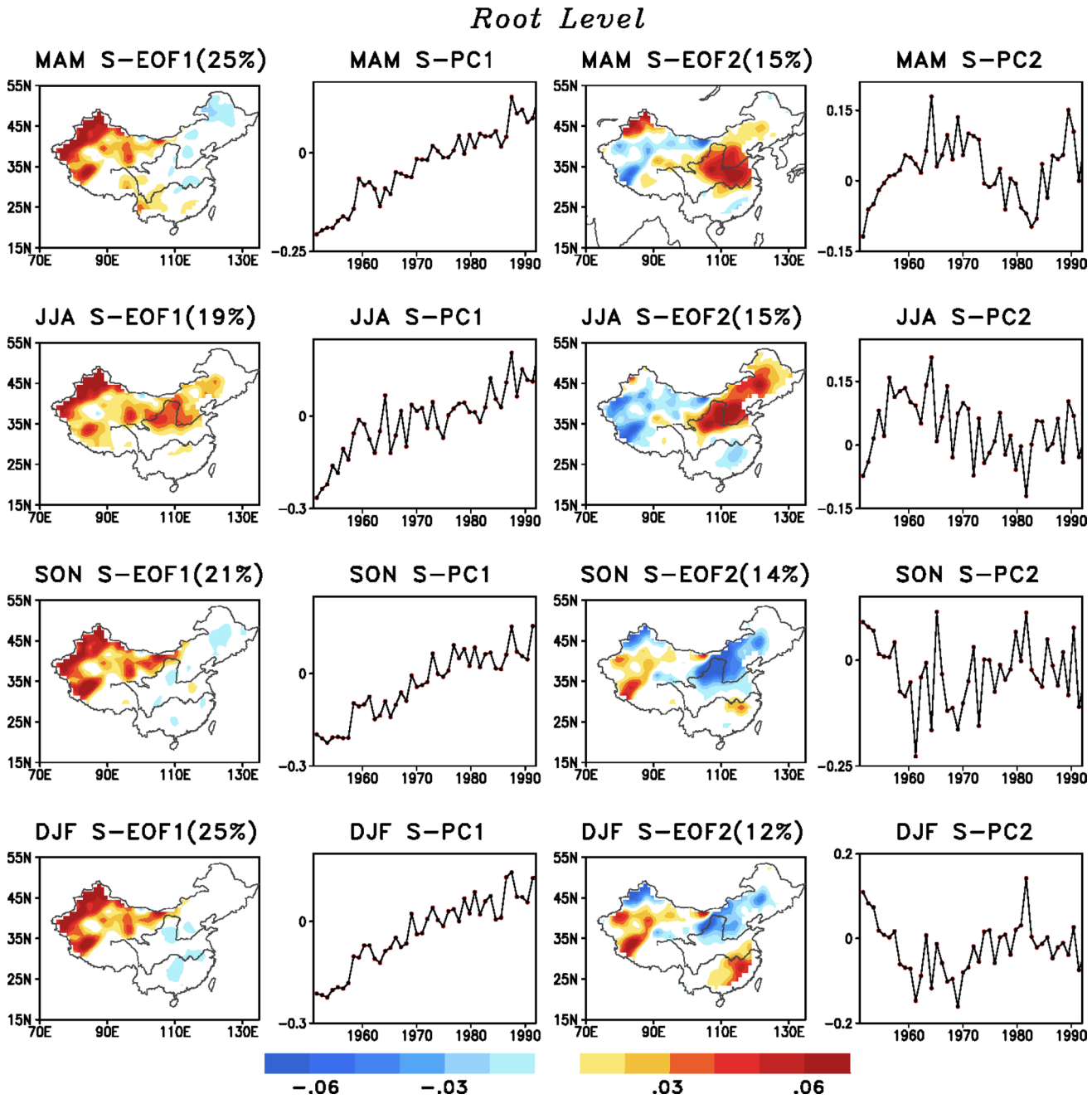

Fig. 15 Same as Fig. 13, but for the root (1.040 m) level

cycle and the spatial distributions of the potential predictability for the seasonal mean soil moisture in the top-1 m soil layer over China has been examined. The potential predictability was generally very good, with lowest value of 0.76 during summer (JJA) and highest value of 0.94 in winter (DJF). The largest predictability was mainly located in the northwest of China; that is in the arid and semiarid areas of China. The potential predictability was lowest over eastern China, in the region most influenced by the EAM.

The analysis showed that the most important source of predictability for the top-1 m soil moisture in China, during MAM–DJF, originated from the soil moisture persistence (comprising more than 50 % of the potential predictability). SST anomalies in the global oceans also contributed sources to the predictability for China soil moisture. Particularly, the SST anomalies in the area of Indian Ocean, the North Atlantic and the eastern tropical Pacific Oceans were well related to the predictable soil moisture modes of MAM, JJA and SON/DJF, respectively. In addition, the

linear trends also served as a source of predictability in all of the four seasons.

Analysis of the covariance of anomalous atmospheric circulation associated with the slow mode indicated that variability in the WPSH played an important role on soil moisture in China. The WPO, NAO and PNA teleconnection patterns were also strongly related to the predictable modes of the seasonal soil moisture in China for MAM, JJA and SON/DJF, respectively.

Based on these findings, we proposed a statistical prediction scheme, using the slow soil moisture PCs as predictands, and using the SSTs, linear trends and soil moisture persistence as predictors. With this S-PC prediction scheme, the prediction skills of soil moisture in China were 59, 51, 62 and 77 % from MAM to DJF, respectively. This was considerable greater than the simple grid prediction scheme, which used the same set of candidate predictors.

The results summarized above are based on analyses of the soil moisture in uppermost 1 m. A critical question is how the potential predictability and predictable signals changes with the depths? To address this question, we have performed the predictability analysis for the soil moisture in different levels as those we have done for the top-1 m. The potential predictability for the soil moisture of top (0.062 m), middle (0.366 m) and the root (1.040 m) levels are compared in Fig. 12. The potential predictability increases with greater soil depths over the whole of China. This is consistent with the conclusion by Fan et al. (2011), in that the variability in the top layer was noisier, in response to short weather events. Spatial and temporal patterns of the most predictable modes of the soil moisture of these three levels are further examined in Figs. 13, 14, 15. While the potential predictability increases with the increase of soil depth, the spatial structure and temporal variability of the most predictable signals for China soil moisture in the three levels are quite similar. The most predictable modes for other levels between the top and the root levels also look quite similar (figure not shown).

In future work, we plan to partition China into several regions and apply this method to predict seasonal soil moisture in each region, for all seasons. In this way, we hope to further improve the prediction skill for soil moisture in specific areas.

Acknowledgments Thanks to the anonymous reviewers for their valuable comments. We also grateful to the editors for their hard work on this manuscript. This work was supported by National Basic Research Program of China (2012CB956203), the National Natural Science Foundation of China for Young Scholar (41405090), the National Natural Science Foundation of China Project (41575087), and the China Special Fund for Meteorological Research in the Public Interest (GYHY201506001).

References

Chang CP, Zhang Y, Li T (2000) Interannual and interdecadal variations of the East Asian summer monsoon and tropical Pacific SSTs. Part II: meridional structure of the monsoon. J Clim 13:4326–4340

Chen Y, Deng H, Li B, Li Z, Xu C (2014) Abrupt change of temperature and precipitation extremes in the arid region of Northwest China. Quat Int 336:35–43

Fan Y, Van Den Dool HM, Wu W (2011) Verification and intercomparison of multimodel simulated land surface hydrological datasets over the United States. J Hydrometeorol 12:531–555. doi:10.1175/2011JHM1317.1

Francis RICC, Renwick JA (1998) A regression-based assessment of the predictability of New Zealand climate anomalies. Theor Appl Climatol 60:21–36

Frederiksen CS, Zheng X (2000) Chaos, potential predictability and model validation of climate variations. Aust NZ Ind Appl Math J 42E:C608–C626

Frederiksen CS, Zheng X (2004) Variability of seasonal-mean fields arising from intraseasonal variability: part2, application to NH winter circulations. Clim Dyn 23:193–206

Frederiksen CS, Zheng X (2007) Coherent patterns of interannual variability of the atmospheric circulation: the role of intraseasonal variability. In: Denier J, Frederiksen JS (eds) Frontiers in turbulence and coherent structures, world scientific lecture notesin complex systems, vol 6. World Scientific, Singapore, pp 87–120

Frederiksen CS, Zheng X, Grainger S (2014) Teleconnections and predictive characteristics of Australian seasonal rainfall. Clim Dyn 43(5–6):1381–1408

Gong D, Ho C (2002) Shift in the summer rainfall over the Yangtze River Valley in the late 1970s. Geophys Res Lett 29(10):1436

Goovaerts P (1997) Geostatistics for natural resources evaluation. Oxford University Press, Oxford, p 467

Grainger S, Frederiksen CS, Zheng X (2009) Estimating the potential predictability of Australian surface maximum and minimum temperature. Clim Dyn 32(4):443–455

Grainger S, Frederiksen CS, Zheng X (2013) Modes of interannual variability of Southern Hemisphere atmospheric circulation in CMIP3 models: assessment and projections. Clim Dyn 41:479–500

Gu W, Li C, Wang X, Zhou W, Li W (2009) Linkage between mei-yu precipitation and North Atlantic SST on the decadal timescale. Adv Atmos Sci 26(1):101–108

He C, Zhou T (2015) Responses of the western North Pacific Subtropical High to global warming under RCP4.5 and RCP8.5 scenarios projected by 33 CMIP5 models: the dominance of tropical Indian Ocean–tropical western Pacific SST gradient. J Clim 28:365–380

Huang R, Sun F (1994) Impacts of the thermal state and the convective activities in the tropical western Pacific warm pool on the summer climate anomalies in East Asia. Sci Atmos Sin 18(2):141–151 **(in Chinese)**

Hunter RD, Meentemeyer RK (2005) Climatologically aided mapping of daily precipitation and temperature. J Appl Meteor 44:1501–1510

Kalnay E, Kanamitsu M, Kistler R, Collins W, Deaven D, Gandin L, Iredell M, Saha S, White G, Woollen J, Zhu Y, Leetmaa A, Reynolds R, Chelliah M, Ebisuzaki W, Higgins W, Janowiak J, Mo KC, Ropelewski C, Wang J, Jenne R, Joseph D (1996) The NCEP/NCAR 40-year reanalysis project. Bull Am Meteorol Soc 77:431–471

Koster RD, Suarez MJ (2001) Soil moisture memory in climate models. J Hydrometeor 2:558–570

Li M, Ma Z (2012) Soil moisture-based study of the variability of dry-wet climate and climate zones in China. Chin Sci Bull 57:531–544
Li M, Ma Z, Du J (2010) Regional soil moisture simulation for Shaanxi Province using SWAT model validation and trend analysis. Sci China-Earth Sci 53(4):575–590
Li M, Ma Z, Niu G (2011) Modeling spatial and temporal variations in soil moisture in China. Chin Sci Bull 56(17):1809–1820
Li B, Chen Y, Chen Z, Xiong H, Lian L (2015) Why does precipitation in northwest China show a significant increasing trend from 1960 to 2010? Atmos Res 167:275–284
Liu Y, Ding Y (1995) Reappraisal of the influence of ENSO Events on Seasonal Precipitation and temperature in China. Chin J Atmos Sci 19(2):200–208 **(in Chinese)**
Ma Z, Wei H, Fu C (2000) Relationship between regional soil moisture variation and climatic variability over east China. Acta Meteorol Sin 58(3):278–287 **(in Chinese)**
Ma Z, Fu C, Xie L, Chen W, Tao S (2001) Some problems in the study on the relationship between soil moisture and climatic change. Adv Earth Sci 16(4):563–568 **(in Chinese)**
Madden RA (1976) Estimates of the natural variability of time-averaged sea-level pressure. Mon Weather Rev 104:942–952
Meng L, Long D, Quiring S, Shen Y (2014) Statistical analysis of the relationship between spring soil moisture and summer precipitation in East China. Int J Climatol 34(5):1511–1523
Nie S, Luo Y, Zhu J (2008) Trends and scales of observed soil moisture variations in China. Adv Atmos Sci 25(1):43–58
Oleson KW, Niu GY, Yang ZL, Lawrence DM, Thornton PE, Lawrence PJ, Stockli R, Dickinson RE, Bonan GB, Levis S (2007) CLM3.5 documentation, technical report, National Center for Atmospheric Research, Boulder, Colo. http://www.cgd.ucar.edu/tss/clm/distribution/clm3.5/
Rayner NA, Parker DE, Folland CK, Alexander LV, Horton EB, Rowell DP (2003) Globally complete analyses of sea-surface temperature, sea-ice and marine air temperature, 1871–2000. J Geophys Res 108:4407
Seneviratne SI, Koster RD, Guo Z, Dirmeyer PA, Kowalczyk E, Lawrence D, Liu P, Lu CH, Mocko D, Oleson KW, Verseghy D (2006) Soil moisture memory in AGCM simulations: analysis of global land–atmosphere coupling experiment (GLACE) data. J Hydrometeorol 7:1090–1112
Seneviratne SI, Corti T, Davin EL, Hirschi M, Jaeger EB, Lehner I, Orlowsky B, Teuling AJ (2010) Investigating soil moisture–climate interactions in a changing climate: a review. Earth Sci Rev 99:125–161
Sheffield J, Wood EF (2007) Characteristics of global and regional drought, 1950–2000: analysis of soil moisture data from off-line simulation of the terrestrial hydrologic cycle. J Geophys Res 112:D17115
Sheffield J, Goteti G, Wen F, Wood EF (2004) A simulated soil moisture based drought analysis for the United States. J Geophys Res 109:D24108
Sheffield J, Goteti G, Wood EF (2006) Development of a 50-year high resolution global dataset of meteorological forcings for land surface modeling. J Clim 19:3088–3111
Shen Y, Xiong A, Wang Y, Xie P (2010) Performance of high resolution satellite precipitation products over China. J Geophys Res 115:D02114
Shi Y, Shen Y, Kang E, Li D, Ding Y, Zhang G, Hu R (2007) Recent and future climate change in northwest China. Clim Change 80:379–393
Shukla J (1983) Comment on ''natural variability and predictability''. Mon Weather Rev 40:581–585
Sun C, Li W, Zhang Z, He J (2005) Distribution and variation features of soil humidity anomaly in Huaihe river and its relationship with climatic anomaly. J Appl Meteorol Sci 16(2):129–138 **(in Chinese)**
Wang B, Li T (2004) East Asian monsoon–ENSO interactions. In: Chang CP (ed) East Asian monsoon. World Scientific, Singapore, pp 177–212
Wang B, LinHo (2002) Rainy season of the Asian-Pacific summer monsoon. J Clim 15:386–398
Wang Y, Zhou L (2005) Observed trend in extreme precipitation events in China during 1961–2001 and associated changes in large-scale circulation. Geophys Res Lett 32:L09707
Wang B, Wu R, Fu XH (2000) Pacific-East Asian teleconnection: how does ENSO affect East Asian climate? J Clim 13:1517–1536
Wang A, Lettenmaier DP, Sheffield J (2011) Soil moisture drought in China, 1950–2006. J Clim 24:3257–3271
Wilks DS (1995) Statistical methods in the atmospheric sciences. Academic Press, Cambridge, p 467
Wu R, Hu Z, Kirtman BP (2003) Evolution of ENSO-related rainfall anomalies in East Asia. J Clim 16:3742–3758
Wu R, Yang S, Liu S, Sun L, Lian Y, Gao Z (2011) Northeast China summer temperature and North Atlantic SST. J Geophys Res 116:D16116
Xu X, Chen H, Zhang F (2007) Temporal and spatial change of vegetation cover in the Northwest of China and factors analysis influencing on vegetation variation. Environ Sci 28(1):41–47 **(in Chinese)**
Ying K, Zheng X, Quan XW, Frederiksen CS (2013) Predictable signals of seasonal precipitation in the Yangtze–Huaihe River Valley. Int J Climatol 33:3002–3015
Ying K, Zhao T, Zheng X (2014) Slow and intraseasonal modes of the boreal winter atmospheric circulation simulated by CMIP5 models. Atmos Ocean Sci Lett 7:34–41
Ying K, Zhao T, Quan XW, Zheng X, Frederiksen CS (2015) Interannual variability of autumn to spring seasonal precipitation in eastern China. Clim Dyn 45(1–2):253–271
Yu R, Zhou T, Xiong A, Zhu Y, Li J (2007) Diurnal variations of summer precipitation over contiguous China. Geophys Res Lett 34:L01704
Zhai P, Zhang X, Wan H, Pan X (2005) Trends in total precipitation and frequency of daily precipitation extremes over China. J Clim 18:1096–1108
Zhan Y, Lin Z (2011) The relationship between June precipitation over mid-lower reaches of the Yangtze River basin and spring soil moisture over the East Asian monsoon region. Acta Meteorol Sin 25(3):355–363
Zhang R, Zuo Z (2011) Impact of spring soil moisture on surface energy balance and summer monsoon circulation over East Asia and precipitation in East China. J Clim 24:3309–3322
Zhang R, Sumi A, Kimoto M (1999) A diadnostic study of the impact of El Nino on the precipitation in China. Adv Atmos Sci 16:229–241
Zhang G, Wu S, Wang Z (2003) The signal of climatic shift in Northwest China deduced from river runoff change in Xinjiang region. J Glaciol Geocryol 25:183–187 **(in Chinese)**
Zhang W, Zhou T, Yu R (2008a) Spatial distribution and temporal variation of soil moisture over China. Part I: multi-data intercomparison. Chin J Atmos Sci 32(2):581–597
Zhang W, Yu R, Zhou T (2008b) Spatial distribution and temporal variation of soil moisture over china part II: the evaluations for coupled models simulations. Chin J Atmos Sci 32(5):1128–1146
Zhao T, Hua L (2009) Applicability evaluation of surface pressure for several reanalysis datasets over China. J Appl Meteorol Sci 20:70–79 **(in Chinese)**
Zhao T, Guo W, Fu C (2008) Calibrating and evaluating reanalysis surface temperature error by topographic correction. J Clim 21:1440–1446

Zhao T, Chen L, Ma Z (2014) Simulation of historical and projected climate change in arid and semi-arid areas by CMIP5 models. Chin Sci Bull 59(4):412–429

Zheng X, Frederiksen CS (1999) Validating interannual variability in an ensemble of AGCM simulations. J Clim 12:2386–2396

Zheng X, Frederiksen CS (2004) Variability of seasonal-mean fields arising from intraseasonal variability: part 1. Methodology. Clim Dyn 23:171–191

Zheng X, Frederiksen CS (2006) A study of predictable patterns for seasonal forecasting of New Zealand rainfall. J Clim 19:3320–3333

Zheng X, Nakamura H, Renwick JA (2000) Potential predictability of seasonal means based on monthly time series of meteorological variables. J Clim 13:2591–2604

Zhou T, Yu R, Li H, Wang B (2008) Ocean forcing to changes in global monsoon precipitation over the recent half-century. J Clim 21(15):3833–3852

Zhou T, Yu R, Zhang J, Drange H, Cassou C, Deser C, Hodson DLR, Sanchez-Gomez E, Li J, Keenlyside N, Xin X, Okumura Y (2009) Why the western Pacific subtropical high has extended westward since the late 1970s. J Clim 22:2199–2215

Zhou T, Hsu HH, Matsuno J (2011) Summer monsoons in East Asia, Indochina, and the western North Pacific. In: Chang C-P et al (eds) The global monsoon system: research and forecast, 2nd edn. World Scientific Publishing Co, Singapore, pp 43–72

Zhou T, Song F, Lin R, Chen X, Chen X (2013) The 2012 north China floods: explaining an extreme rainfall event in the context of a long-term drying tendency. In: Explaining extreme events of 2012 from a climate perspective. Bull Am Meteorol Soc 94(9):S49–S51

Zuo Z, Zhang R (2007) The spring soil moisture and the summer rainfall in eastern China. Chin Sci Bull 52:3310–3312

Zuo Z, Zhang R (2009) Temporal and spatial features of the soil moisture in boreal spring in eastern China. Sci China Earth Sci 52(2):269–278

Zuo J, Li W, Ren H, Chen L (2012) Change of the relationship between spring NAO and East Asian summer monsoon and its possible mechanism. Chin J Geophys 55:23–34 **(in Chinese)**

Zuo J, Li W, Sun C, Xu L, Ren H (2013) Impact of the North Atlantic sea surface temperature tripole on the East Asian summer monsoon. Adv Atmos Sci 30(4):1173–1186